Preparation and characterization of a gold nanoparticle/graphene composite for the electrocatalytic oxidation of glucose

Åbo Akademi University

Faculty of Science and Engineering

Raegan Chambers

Master's Programme in Excellence in Analytical Chemistry

Degree Project in Analytical Chemistry, 30 credits

Supervisor: Rose-Marie Latonen (Åbo Akademi University)

Co-supervisor(s): Agnes Heering (University of Tartu)

Jaypee Oña (Åbo Akademi University)

Sara Lund (Åbo Akademi University)

June 2022

i.Preface

This Master's thesis was done at Åbo Akademi University in collaboration with the University of Tartu as part of the *Excellence in Analytical Chemistry* program - an Erasmus Mundus joint degree program. The research for this thesis was carried out at the Laboratory of Molecular Science and Engineering at Åbo Akademi University in Turku, Finland during the 2021 – 2022 academic year.

I would like to thank my supervisor at Åbo Akademi University Dr. Rose-Marie Latonen who graciously took the time and effort to help guide me through the writing process and provided helpful insights throughout the entirety of the process. My co-supervisor at Tartu University Dr. Agnes Heering who aided during the writing process of this thesis. My co-supervisors at Åbo Akademi University Sara Lund and Jaypee Oña both of whom humbly mentored me throughout the entirety of this work. Without the constant support of my supervisors this Master's thesis would not be what it is and I will be forever grateful for them.

I would like to thank Dr. Johan Bobacka, Dr. Ivo Leito and Dr. Anu Teearu-Ojakäär for their constant support throughout the entirety of the EACH program and for all the work they put into making our experience with the program as close to normal as they possibly could given the current situation.

Finally, I would like to thank my fellow EACH colleagues. These past two years have been filled with uncertainties; throughout lockdown we were able to forge close friendships and become a family. Specifically, to my EACH colleagues at Åbo Akademi University, the constant comradery will forever be some of my greatest memories; the late night writing parties that we endured to the adventures we took a part in are forever close to my heart. Thank you all for pushing me to be the best version of myself.

While the last two years have been filled with uncertainty as a result of COVID and plans were constantly being reworked, I am forever thankful for the opportunity to be a part of the *Excellence in Analytical Chemistry* program.

ii. Abstract

Over the past few years there has been a shift towards sustainably producing chemicals. The valorization of biomass into value-added chemicals has been thoroughly investigated as a means of production for several carbon containing compounds. Through the use of lignocellulose waste materials, glucose can be obtained and electrochemically oxidized to gluconic acid. Oxidation is enhanced using graphene/gold nanoparticle (AuNPs) electrocatalyst. Electrocatalysts offer an advantage over the current industrial process of fermentation. The waste associated with fermentation requires proper disposal in order to be compliant with environmental safety. The use of an electrocatalyst also holds an advantage over chemical oxidation as it provides a less harsh chemical environment and can be ran under ambient conditions. In order for the catalyst to be viable for industrial use it must have high activity, be selective towards the formation of gluconic acid and be stable. In this research, a stable water-based graphene dispersion fabricated by high shear exfoliation method was used as a support for AuNPs prepared by the pH- controlled addition of a hydrogen tetrachloroaurate (III) hydrate precursor and was spray-coated on a glassy carbon (GC) electrode and drop-casted onto a carbon felt (CF) electrode. Carbonous electrode materials were used in this work as they provide are a high surface area substrate. AuNPs were used over other noble metal catalysts as they have been shown in literature to selectively oxidize glucose at lower potentials than both copper and platinum catalysts. The graphene/AuNPs composite and films were physico-chemically, electrochemically and microscopically characterized. Following the electrochemical impedance spectroscopy (EIS) and cyclic voltammetry (CV) experiments the graphene/AuNPs film on the GC electrode degraded. Thus, for the determination of the activity and stability of the graphene/AuNPs catalyst, a CF substrate was used. Electrolysis of glucose on the graphene/AuNPs CF electrode produced gluconic acid as confirmed by high performance liquid chromatography (HPLC). The stability of the electrode was analyzed over four, three-hour electrolysis by looking at the resulting chronoamperogram, the glucose conversion efficiency and the turnover frequency. As the electrolysis was carried out using the same electrode the stability could be analyzed. The average glucose conversion efficiency of the four electrolysis was 18 % and the average TOF was $1.97 \cdot 10^3$ h^{-1}. The graphene/AuNPs CF electrode was determined to be stable and a viable option for the electrochemical oxidation of glucose to gluconic acid.

iii. Table of Contents

iv. List of abbreviations and symbols

4PP: 4-Point Probe Conductivity

A: absorbance

AC: Alternating Current

AFM: Atomic Force Microscopy

AuNPs: Gold Nanoparticles

b: path length

B.E.T.: Brunauer-Emmitt-Teller

c: concentration

C: capacitance

CE: Counter Electrode

CF: Carbon Felt

CNTs: Carbon Nanotubes

CV: Cyclic Voltammetry

E: potential

ECO: Electrocatalytic Oxidation

EDS: Energy Dispersion X-Ray Spectroscopy

EIS: Electrochemical Impedance Spectroscopy

f: frequency

$f_{2:}$ finite width correction factor

GC: Glassy Carbon

i: current

I: bias current

ICP: Inductively Coupled Plasma

IUPAC: International Union of Pure & Applied Chemistry

k: rate constant

LPE: Liquid Phase Exfoliation

N: rotor speed

OES: Optical Emission Spectroscopy

P: transmitted light

P_0: incident light

R: universal gas constant

RE: Reference Electrode

SC: Sodium Cholate

SEM: Scanning Electron Microscopy

t: film thickness or time

T: transmittance or temperature

TEM: Transmission Electron Microscopy

UV: Ultraviolet

V: voltage

Vis: Visible

WE: Working Electrode

Z: impedance

α: transfer coefficient

δ: thickness

ε: extinction coefficient

v: scan rate

σ: conductivity

ρ: resistivity

φ: phase

1 Introduction

As sustainability has emerged as a new focal point in industry, a shift towards the sustainable production of materials has been introduced. The valorization of biomass into value-added chemicals has been suggested as a sustainable means of production for several carbon containing compounds. The use of biomass as a material offers a unique advantage as it allows for the use of waste materials to obtain valuable starting materials. This is exemplified by the acquisition of such starting materials from lignocellulose waste materials. Lignocellulose is composed of three categories of compounds: cellulose, hemicellulose and lignin. It is through the derivation of hemicellulose that glucose can be obtained.[1] Glucose is a valuable starting material as it can be oxidized to gluconic acid – a multi-purpose high value chemical. The use of lignocellulose waste from the forest and paper industries is a more sustainable practice than the use of biomass intended crops as it does not require the use of arable land.[2]

The method of valorization examined in this study was the electrocatalytic oxidation of glucose using a graphene/AuNPs CF electrode. Catalysts are used in the electrochemical oxidation to lower the activation barrier of the reaction.[3,4] By doing this it allows for the overall reaction conditions to be less harsh than in a electrochemical reaction ran without a catalyst.[5] The electrocatalytic oxidation of glucose can be carried out using noble metal nanoparticle catalyst such as platinum or gold. The use of AuNPs allows for a higher overall catalytic activity and better selectivity.[6,7] This is attractive for the scalability and implementation of electrocatalytic oxidation of glucose to gluconic acid in an industrial setting as the catalyst needs to be selective, active and stable.[3,8] The AuNPs were supported on graphene flakes that were shear force exfoliated from graphite. Water based shear force exfoliation produces a stable graphene/sodium cholate (SC) dispersion in a mild chemical environment and thus is attractive for the scalability of graphene production. The use of SC kept the graphene sheets from amalgamation.[9] The use of carbon felt allows for a strong adhesion of the graphene/AuNPs composite onto the electrode. Carbonous material as both a support and substrate offers high surface area and mechanical stability of the electrode.[10,11]

The graphene/AuNPs composite was characterized using a multitude of techniques. The presence of graphene flakes was confirmed via SEM and TEM. TEM was also used to determine the average AuNP particle diameter. The surface area of the graphene/AuNPs carbon felt electrode was determined via nitrogen physisorption. The gold content in the composite was analyzed via ICP-OES and SEM-EDS. The electrochemical properties were investigated using CV and EIS. The CV confirmed oxidation of glucose

occured solely on the electrode containing the AuNPs. Following the 3-hour electrolysis the amount of gluconic acid was determined via HPLC. This value was also used to analyze the stability and overall activity of the graphene/AuNPs CF electrode.

2 Theory

2.1 Conversion of Biomass

As the impact that the use of hydrocarbons in both the chemical and energy sectors has on the environment is being fully assessed - there has been an increase in interest of the sustainable production of said materials. Hydrocarbons are used in the energy sector due to their ability to transmit and store energy.[12] In May of 2022 the United States had a field production of hydrocarbon gas liquids of 187,173 thousand barrels.[13] Thus cementing the fact that hydrocarbons play an important role in the economy. The current production methods of obtaining hydrocarbons through the use of fossil fuels has led to both socioeconomic and environmental concerns.[14] Obtaining biomass from lignocellulose materials and transforming it into value-added chemicals offers both a lower cost and lower environmental impact alternative.[1]

While the conversion of biomass does provide an alternative route to the production of value-added chemicals, there are socioeconomic concerns that need to be discussed. One major concern is the use of arable land for the production of biomass crops. As the acreage of land used to produce biomass crops increases the amount of land available for food crops decreases. This increases competition for available land and increases the overall price of food.[2] As food security is a growing concern, it is paramount that the socioeconomic drawbacks of biomass crops be thoroughly investigated. One way to mitigate these concerns is to use lignocellulose waste. This can come from waste products arising from agricultural residues, grasses and forestry.[1] Lignocellulose material consists of cellulose, hemicellulose and lignin, and can be converted into a variety of fuels and value-added chemicals. [14] Hemicellulose contains many monosaccharides including glucose which can then undergo further valorization. [15]

2.2 Valorization of Glucose into Gluconic Acid

Glucose is the most abundant monosaccharide.[16] Glucose can be valorized into the value-added weak acid gluconic acid (Figure 1). Due to its ability to dissolve various oxides and carbonates, gluconic acid can be

used to remove rust, grease, paint and other substances without causing damage to the surface underneath.[8]

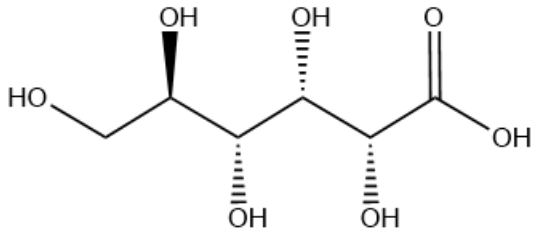

Figure 1: Molecular structure of D-Gluconic Acid.

The annual production capacity of gluconic acid is 60,000 tons. The main production mechanism is glucose oxidation.[8] The oxidation of glucose was first discovered in 1870 and has since expanded to include various methods such as electrochemical, electrocatalytic and biotechnological.[8] The biotechnological processes include fermentation, microbe-assisted oxidation and enzyme-assisted oxidation.[8,17] The most common industrial production method for gluconic acid is the aerobic fermentation of glucose using *Aspergillus niger*.[8,18,19] However, this technique includes environmental drawbacks such as those concerning the disposal of waste materials.[20] Thus in order to improve the sustainability, other production methods have been investigated.

The chemical oxidation of glucose is not a preferred method of production as it tends to produce low yields with limited selectivity that result in undesirable by-products making the isolation of gluconic acid difficult.[8] The chemical oxidation of glucose involves harsh reaction conditions such as the need for high temperatures and high pressure.[6] Electrochemical methods mitigate the need for a harsh environment throughout the bulk of the solution.[5] The difference in the bulk solution and the area surrounding the electrode can be explained by the Nernst Diffusion Layer.[3] The Nernst Diffusion Layer is the region in the electrochemical cell where the species concentration differs between the bulk solution and near the electrode - thus resulting in a difference of reaction conditions. The thickness (δ) of this layer can be

represented graphically (Figure 2) as the intersection of the tangent lines of the bulk concentration (C_b) and the concentration near the electrode (C_e).[21]

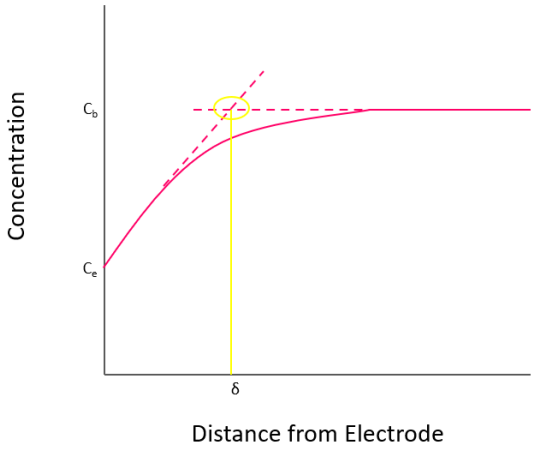

Figure 2: Graphical representation of the thickness of the Nernst Diffusion Layer as its related to the concentration difference near the electrode and bulk of the solution.

Electrochemical methods can also increase the selectivity of the reaction.[19] However, due to electrical costs associated with running electrochemical reactions under optimal conditions, these methods do not pose as an alternative route for the valorization of glucose into gluconic acid on an industrial scale.[8] Electrocatalysts offer a multitude of advantages such as enhanced selectivity towards a specific product and the availability to run the reaction at ambient conditions.[5,6,22] Thus electrocatalytic methods provide a viable alternative to fermentation for the industrial production of gluconic acid.

2.3 Electrocatalyst for the Oxidation of Glucose to Gluconic Acid

Electrochemical reactions can be complex and have slow kinetics as a result of multi-step processes.[3,5] The reaction kinetics can be improved with the use of a catalyst. A catalyst works by providing an alternate pathway for the reaction to occur. This alternative pathway has a lower activation energy than the original one.[3,4] An electrocatalyst can either be a single metal catalyst, a bifunctional catalyst or a transition metal catalyst and is generally located either in the electrolyte solution or on the electrode itself.[3,23] Transition metals catalysts offer a unique opportunity, as the formation of the bonds with the adsorbate occurs among their d-orbitals.[3] This is interesting as it allows for the high-density spin states to be localized around the Fermi level and thus further lowering the activation barrier.[24]In order for the catalytic process to be applicable for industry it must be selective towards the target reagent, have a high catalytic activity, and be mechanically stable over a long period.[3,8]

The catalytic ability of both palladium (Pd) and platinum (Pt) towards the oxidation of glucose has been thoroughly investigated. Both metals result in the deactivation of the catalyst as well as produce unwanted by-products. One way to overcome these drawbacks is to add bismuth (Bi) to the catalyst. However, due to the toxicity of Bi if the end product is to be used in the food and drink industry, this is not a viable alternative.[25] Thus leading to the investigation of the use of other noble metals as a catalyst such as copper and gold.[6,7] The use of a copper catalyst results in the cleavage of carbon-carbon bonds and in the formation of low mass carboxylic acids.[7] The oxidation potential required for glucose using a copper catalyst is at more positive potentials than both the platinum and gold catalyst.[7] Thus, leading to the investigation of a gold catalyst for the oxidation of glucose into gluconic acid.

The oxidation of glucose into gluconic acid follows a similar reaction mechanism for both gold and platinum catalysts.[6] However, the oxidation of glucose on a gold catalyst occurs at lower potentials and provides higher selectivity towards the production of gluconic acid.[6,7] When the electrochemical reaction is carried out in an alkaline solution, both the currents and the activity of the gold electrocatalyst are greatly enhanced as compared to the platinum catalyst.[7] One drawback to the use of gold as an electrocatalyst is the surface poisoning that occurs due to the adsorption of gluconic acid and its analogues onto the electrode surface.[23,26] This tendency towards surface poisoning is greatly reduced through the use of gold nanoparticles (AuNPs).[26]

Carbon-based materials are used as both electrodes and support material for AuNPs, as they offer high specific surface area, and good mechanical, chemical and thermal strength.[10,11] Using an electrode with a high surface area is important as it increases the kinetics of the reaction.[5] Glassy carbon (GC) is an interesting electrode material as it has high thermal stability, strong chemical inertness and is hydrophobic.[27] However issues with the adhesion of films onto a GC electrode have been reported. This can be attributed to its smooth surface and hydrophobicity.[17] Carbon felt (CF) is another carbon material that is used as an electrode due to its high surface area. Two allotropes of carbon are of particular interest for the use of supports for catalytic reactions: carbon nanotubes (CNTs) and graphene. CNTs offer the unique advantage of having a three-dimensional structure. This allows for a greater number of electroactive sites as compared to the graphene.[28] However, graphene does not have metallic impurities a has greater availability. Thus increasing its usability over CNTs.[29]

2.4 Exfoliation of Graphite

Graphite is an allotrope of carbon that consists of sheets of sp^2 hybridized carbon rings. These sheets of carbon rings are graphene.[30] The sheets of graphene are stacked together and held in place by van der Waals forces. While the carbon rings within the sheets are held together by covalent bonds.[31] The force holding the carbon rings together is stronger than the force holding the graphene sheets together. When the conductivity of the graphite is measured parallel to the graphene sheets there is an increase in conductivity versus when the conductivity is measured perpendicular to the sheets. This increase in conductivity can be attributed to the fast movement of electrons among the pi molecular orbitals in the carbon rings.[31]

Graphene was first split from graphite in 2004 via micromechanical cleavage.[32] Innovations in the production of graphene from graphite have led to an increase in the amount of techniques that can be employed; one technique that has been introduced is liquid phase exfoliation (LPE) which includes shear exfoliation, sonication and wet ball milling.[33,34] Wet ball milling is an industrial technique used for the production of various nanoparticles – thus making it a viable option for the scalable exfoliation of graphite. It involves dispersing graphite in a solvent and milling it for an extended period of time. The solvent is then dissolved, and a graphene powder is left.[34] The sonication of graphite is an exfoliation method that employs the use of soundwaves to extract the graphene.[35] The graphite is dispersed and sonicated in a solvent with a small net energetic cost, either an organic solvent or water stabilized with a surfactant, and results in graphene.[36,37] However, sonication is an not easily scalable due to it being energy intensive.[33]

Another method that is scalable, can be employed in an industrial setting and shown to produce a high concentration of few layer graphene is shear exfoliation.[33] Shear exfoliation employs the use of a rotor-stator to induce the separation of the graphene sheets from graphite due to shear force. In this method, the graphene sheets are physically pulled apart from the graphite flakes via kinetic energy. One model that explains how this happens is the shear-induced interlay sliding model. This model employs a difference of velocity in the movement of the liquid at the top and the bottom of the graphite to remove the graphene layers.[38] Shear exfoliation is dependent on a multitude of factors that involve the rotor- stator geometry.[39] Graphene will reaggregate back to graphite if a surfactant, such as sodium cholate (SC), is not added to the solution. The electrostatic properties of SC stabilizes graphene through repulsion. [9,40] However, SC can hinder the conductivity of the dispersions and thus caution should be taken to remove excess SC.[41]

2.5 Characterization Techniques

2.5.1 Ultraviolet – Visible Spectroscopy

UV-Vis spectroscopy is used to measure the amount of radiation that a solution absorbs within the ultraviolet (UV) and visible (vis) region. This region ranges in wavelength from 180 nm to 780 nm.[42] The absorption of radiation is measured using a UV-Vis spectrometer. In this instrument a light source emits radiation within a given range. This radiation is then narrowed down to a single wavelength using either a filter or a monochromator – a filter requires more manual work as it needs to be changed depending on the needed wavelength whereas a monochromator uses an automated process. Once the light has been narrowed down to a given wavelength, the path it takes to the sample is dependent on whether the instrument is single beam or double beam. In a single-beam instrument the sample cells and reference cells must be moved in order to be irradiated by the light. As the intensity of the light can shift within a given moment, this can cause instrumental drift between the measurement of the reference cell and the sample cell. Thus, to obtain a more accurate measurement a double-beam instrument can be used. This instrumentation ensures that the same radiation is being used for both the sample cell and the reference cell.[43] A diagram of a double beam instrument can be seen in Figure 3.

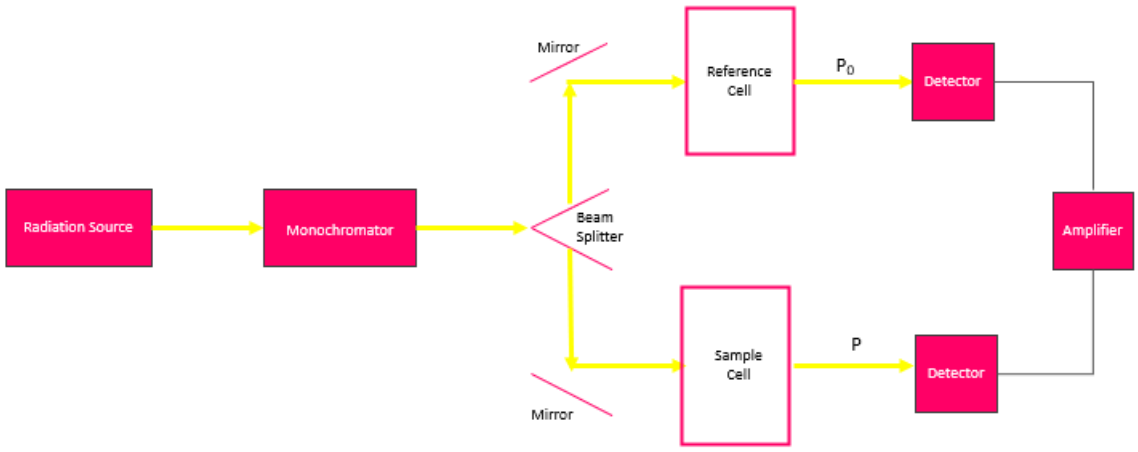

Figure 3: A diagram of a double beam UV-Vis spectrometer. The yellow lines indicate the movement of radiation, *P* is the transmitted light and P_0 is the incident light. The black lines indicate the movement of electrical signal.

Attenuation of the radiation may occur due to several factors – one of such being the scattering of light.[43] In order to compensate for this the absorbance is recorded as a ratio of the incident light and the transmitted light – or the ratio of the light absorbed by the reference cell and the sample cell. The relationship can be explained through Beer-Lambert's Law (Equation 1):

$$A = -\log(T) = \log\frac{P_0}{P} = \varepsilon bc \quad (1)$$

This equation takes into account that the measured absorbance (*A*) is logarithmically related to the transmittance (*T*) or the ratio of the incident light (P_0) over the transmitted light (*P*) which is all equal to the product of the extinction coefficient (ε), the path length of the cell (*b*) and the concentration of the analyte in the solution (*c*). The extinction coefficient is related to how strongly the analyte absorbs radiation – it is dependent on the wavelength used, concentration of the analyte and the analyte itself.[44] For graphene this value was determined to be 6590 mL · mg^{-1} · m^{-1}.[33] By convention the absorbance of a graphene solution is recorded at 660 nm. This is done to keep continuity and allow for accurate comparisons to be made across literature. This is slightly different than in a conventional UV-Vis where the measurement is recorded at the maximum of the absorbance spectra.

2.5.2 Nitrogen Physisorption

The pore size, pore distribution and specific surface area of a sample can be determined via nitrogen physisorption.[45,46] In this technique, the change in relative pressure is correlated to the amount of nitrogen that was adsorbed onto the sample through the thermodynamically reversible process of physisorption.[46] The Brunauer-Emmitt-Teller (B.E.T.) theory allows for an approximation of the pore size and distribution as well as the overall specific surface area of a sample. The B.E.T. method is an approximation as it does not take into account the attractions of the lateral molecules onto the absorbate and makes several assumptions regarding the formation of the monolayer onto the surface of the sample.[45]

2.5.3 Energy Dispersive X-Ray Spectroscopy

Energy dispersive X-Ray Spectroscopy (EDS) is an elemental spectroscopy technique. In EDS, the sample is irradiated by an electron source. In the case of this experiment, EDS was coupled with a scanning electron microscope (SEM) and the sample was irradiated by the SEM's electron beam. The irradiation causes an inner shell electron to be released. Leaving behind a hole which is filled with an electron from a higher energy shell. This shift in electrons releases energy in the form of a characteristic x-ray: thus allowing for the elemental composition of the sample to be determined.[47] When EDS is coupled with SEM almost all of the x-ray photons are measurable.[48] When a sample is irradiated with a high energy source, multiple interactions occur which release different types of energy; such as secondary electrons, Auger electrons, x-rays and sometimes light photons.[49] In EDS the heavier the element the greater the chance that an x-ray photon will be released. Thus the accuracy of EDS improves as the atomic weight of the element increases.[47]

2.5.4 Inductively Coupled Plasma – Optical Emission Spectroscopy

Inductively coupled plasma – optical emission spectroscopy (ICP-OES) is an elemental spectroscopy technique. In ICP-OES the sample is excited via plasma. The plasma is hot enough (7000 K) that it can excited almost all of the elements. The plasma is usually generated by argon gas that undergoes inductive coupling. Inductive coupling occurs due to the collision of the charged argon species with the neutral argon atoms occurs. It is based on the frequency applied to it by electromagnetic induction.[50] Once the sample has been excited to a higher energetic state it relaxed back down. As it relaxes down it emits characteristic radiation.[42] It is due to this that ICP-OES can be used to analyze samples with multiple analytes.[51] ICP-OES is an extremely selective technique and can be used to investigate trace concentrations of analytes.[51,52]

2.5.5 Transmission Electron Microscopy

Transmission Electron Microscopy (TEM) is a microscopy techniques that can be used both qualitatively and quantitatively.[53] In TEM a well-defined electron beam is focused onto a sample that is usually less than 100 nm thick.[54] When the electrons pass through the sample, they are then directed onto a fluorescent plate. An image is produced which correlated to the kinetic energy of the electrons hitting the plate. The kinetic energy is a direct correlation to the density of the sample.[55]

2.5.6 Scanning Electron Microscopy

Scanning electron microscopy (SEM) is a microscopy technique that investigates the morphography of a sample. In SEM an electron beam is focused onto a sample – the sample can range in size from being thin to a bulk sample.[56] The beam penetrates about 1 µm and releases secondary electrons.[49] As the beam is scanned across the sample, the amount of secondary electrons being released from the sample changes. The resulting image is formed based on the number of electrons that reach the detector.[49] This is ultimately a result of the change in distance between the electron beam and the sample surface.[57]

2.5.7 Atomic Force Microscopy

Atomic force microscopy (AFM) is a microscopy technique that focuses on the difference of height to form a topological image of the surface of a sample[58]. The AFM tip is connected to a cantilever beam which is scanned across the sample. As the tip interacts with the sample it is deflected.[59] A laser is focused on the cantilever and reflects the beam back to a photodiode; resulting in an image.[58] An image is formed as the result of the difference in height of the sample. Convention has it that the lighter regions of the image are a result of the taller regions on the sample and the darker regions represent shorter regions. AFM can be used to determine the thickness and roughness of thin films with high accuracy.[54,56,58]

2.5.8 4-Probe Conductivity Technique

4-point probe conductivity (4PP) is used to determine the conductivity of a thin film via resistivity measurement. In this form of conductivity measurement, 4 equally spaced probes are placed in a linear configuration and placed on the film. A known current is passed through the outer two probes while the resulting decrease in voltage is measured across the inner two probes as shown in figure 4.[60]

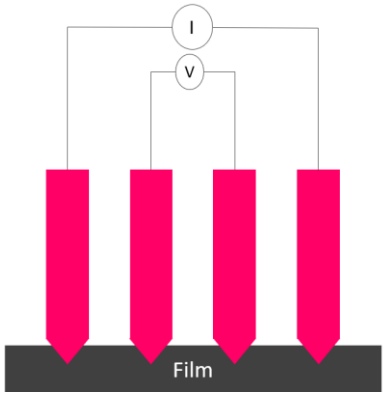

Figure 4: A diagram of the 4PP instrumentation.

The conductivity (σ) of the films is calculated using equations 2 and 3:[61]

$$\rho = \frac{\pi}{\ln(2)} t \frac{V}{I} f_2 \tag{2}$$

$$\sigma = \frac{1}{\rho} \tag{3}$$

The resistivity (ρ) of the films can be calculated using equation 3. In this study the film thickness (t) was measured via AFM, voltage (V) was recorded from the instrument, the bias current (I) was 1 mA and the correction factor for finite width (f_2) was found using the diagram provided by Smits.[61] The conductivity was then calculated by taking the reciprocal of the resistivity.

2.5.9 Electrochemical Impedance Spectroscopy

Electrochemical Impedance Spectroscopy (EIS) is a technique that is used to measure the impedance of an electrochemical system. The impedance of a system represents the resistance it has towards a current.[62] The impedance is measured using the phasor approach. In this approach a sinusoidal alternating current (AC) is applied to the system. The resulting currents (i) and voltages (V) can be represented as vectors using an Argand diagram (Figure 5).[3] The current resulting from the sinusoidal AC will also be sinusoidal and have the same frequency (f) as the voltage. However, the current wave is usually out of

phase (φ) from the voltage wave and can have a different amplitude. By adding in components for the resistor and capacitor and showing the voltage across the two, the impedance (Z) of the cell can then be calculated. [3]

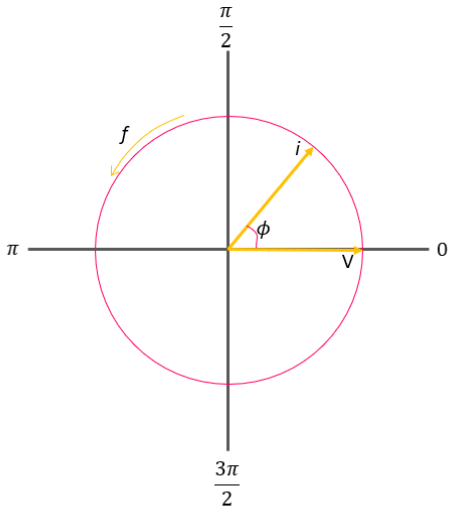

Figure 5 : Argand diagram of an applied AC potential and the current.

By looking at the results from the EIS the capacitance (C) of the system can be measured using equation 4. This is done by using the impedance at the lowest frequency (f). Most of the impedance at this frequency is a result of the capacitor.[43]

$$C = \frac{1}{2\pi f(-Z'')} \qquad (4)$$

2.5.10 Cyclic Voltammetry

Cyclic voltammetry (CV) is used to measure electrochemical process taking place in a solution at various potentials. A CV is recorded using a potentiostat. A potentiostat is used as it allows for control of the potential between the working and reference electrodes.[3] The most common set up to be used with the potentiostat in the measurement of an electrochemical processes is a 3-electrode set up; consisting of a working electrode (WE), a counter electrode (CE) and a reference electrode (RE). A diagram of a 3-electrode system can be seen in Figure 6. The electrochemical reaction of interest is usually carried out on the WE. The current is carried between it and the CE. It is important that the RE has a known potential and does not participate in the reaction. Through the RE that we can determine the potential of the WE.[63]

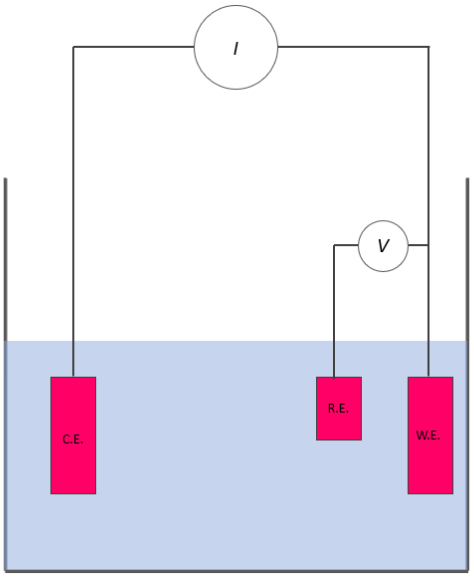

Figure 6: A schematic of a common 3- electrode electrochemical cell setup.

In a CV the scan starts at a given potential and moves to a second before returning back to the starting potential. This is done in an organized manner such that the scan follows a specific scan rate.[43] The electrochemical measurements recorded are a direct result of the electron transfer processes happening at the electrode surface. As the potential is changed so too is the concentration of the species at the electrode surface. As more species is concentrated at the electrode surface there is a rise in a current, resulting in a peak on the voltammogram.[3] The current measured can come from two different processes: capacitive current or Faradic current. Faradaic current is a current arising from an electron transfer process. Capacitive current is a result of the formation of an electrical double layer and not an electron transfer process taking place. [63]

A CV can be used as a qualitative tool to determine the reaction mechanisms taking place within a given reaction cell. Mechanistically a CV can show different processes such as adsorption and deposition. These

are determined based on the resulting shape of the CV. The shape of the CV can also be used to determine if the electrochemical process is reversible or irreversible.[3] There are two common conventions used for displaying the resulting CV – the American convention and the International Union of Pure & Applied Chemistry (IUPAC) convention. Using the American convention: the high potentials are on the left side of the CV; low potentials are on the right side; the oxidation peak is on the bottom of the graph; while the reduction peak is on the top of the graph. Using the IUPAC convention: the low potentials are on the left side of the CV; high potentials are on the right side; the oxidation peak is on the top of the graph; while the reduction peak is on the bottom of the graph.[64]

An electrochemical system can be described as either reversible or irreversible. In a reversible system, Nernstian equilibrium is always observed, and the cathodic potential is not dependent on the sweep rate. However, in an irreversible system the observed potential is dependent on the sweep rate. This relationship is described by equation 5:

$$E_p^C = K - \frac{2.3\,R\,T}{2\alpha_C n_\alpha F}\log(\upsilon) \qquad (5)$$

Where the cathodic potential ($E_p{}^C$) is equal to the rate constant (K) minus the quotient of the universal gas constant (R) and the temperature (T) over the cathodic transfer coefficient (α_C) times the logarithmic function of the scan rate (v).

3 Experimental

3.1 Chemicals

Three different types of graphite were used in the optimization of the graphene dispersion: one was from Sigma-Aldrich and had a flake size of more than 150 µm; the second was natural flake graphite from Haapamäki, Finland, with a flake size ranging from up to 1 mm; and one was commercial graphite from Alfa Aesar with a flake size of less than 45 µm. The graphite from Alfa Aesar was decided to be used throughout the rest of the work due to its availability in the lab. The sodium cholate (SC) powder was obtained from Acros Organics. Hydrogen tetrachloroaurate (III) hydrate from Alfa Aesar as supplied from ABCR GmbH was used in the loading of the AuNPs. Sodium hydroxide from Merck KGaA was used as electrolyte salt in the electrocatalytic oxidation experiments. D (+) – glucose anhydrous from Fluka was used for all solutions containing glucose. D (-) – fructose from Sigma and sodium gluconate from Sigma-Aldrich were used for the creation of calibration solutions for the quantification of analytes. Deionized MilliQ water with a resistivity of 18 MΩ·cm was used throughout this work.

3.2 Preparation of Graphene Dispersions

3.2.1 Preparation of Sodium Cholate and Graphene Dispersion for Preparation of Electrode

A 5.00 mM SC solution was prepared by weighing 2.16 g of SC powder that had previously been dried overnight at 100 °C and dissolving it in water in a 1.00 L volumetric flask; 30.00 mL of the 5.00 mM SC solution was combined with 3.00 g of graphite in a 100 mL borosilicate glass bottle. The shear-exfoliation was carried out using a POLYTRON® immersion disperser with a PT 10-35 GT drive unit coupled with a PT-DA 20 dispersing aggregate. The rotor head was positioned inside the 100 mL borosilicate glass bottle. The mixing time (*t*) was 3 h with a rotor speed (*N*) of 22000 RPM. To help with the foaming of the dispersion, the rotor speed was gradually increased until 22000 RPM and then held constant throughout the exfoliation. The exfoliation was kept at a constant temperature of 10.0 °C using a temperature regulation system with a MGW Lauda MT bath circulator and Hetofrig water bath cooler. The dispersion was centrifuged using a Hermle LaborTechnik Bedienungsanleitung für Tischkühlzentrifuge Z36HK for 30 min at 221.21 RPM corresponding to a RCF of 270 G, the supernatant was transferred into a new centrifuge tube and centrifuged again for 30 min at the same rotation speed. Following centrifugation, a UV-Vis measurement was recorded. The dispersions were dialyzed for 2 h under magnetic stirring using Spectra/Por® 3 dialysis membranes with a molecular weight cutoff of 3500 Da to remove the excess SC. The volume ratio of the sample and the dialysate was 1:300. A UV-Vis measurement was recorded following the dialysis to confirm the final graphene concentration.

3.2.2 Preparation of Cellulose Nanocrystals and Graphene Dispersions

CNC was used as a stabilizer for the graphene sheets instead of SC. Prior to the exfoliation two different cellulose nanocrystal (CNC) dispersions were prepared in the Laboratory of Natural Materials Technology. Due to the availability of the CNC dispersion in the lab, two different CNC dispersions were used. One was hydrolyzed in sulfuric acid (64 %) for 1.5 h and the other for 2.0 h – by altering the hydrolysis time, the amount of anionic sulphate half-ester groups that were formed on the CNC was altered. It has been shown that the difference in the two hydrolysis times does not have an effect on the final graphene concentration.[33] For the exfoliation where the CNC underwent 2 h hydrolysis: 3.00 g of graphite, 8.66 mL of the CNC solution and 21.34 mL of water was combined in a 100 mL borosilicate glass bottle. For the exfoliation where the CNC underwent 1.5 h hydrolysis; 3.00 g of graphite, 8.94 mL of CNC solution and 21.06 mL of water was combined in a 100 mL borosilicate glass bottle. For all dispersions, the mixture was shear-exfoliated using the same mixer as for the graphene/SC dispersions. The rotor head was positioned inside a 100 mL borosilicate glass bottle. The mixing time (*t)* was 3 h and the rotor speed (*N)* was 22000 RPM. For the dispersion where the CNC underwent 2 h hydrolysis the temperature (*T)* was 15.0 °C and for the dispersion where the CNC underwent 1.5 h hydrolysis the temperature (*T*) was kept at 18.0 °C. The change in temperature had no effect in the final graphene concentration[33]; but did reduce the overall energy consumption of the exfoliation. To decrease foaming during the exfoliations, the rotor speed was gradually increased until the final speed was reached and then held constant for the duration of the exfoliation. A constant temperature was kept throughout the exfoliation process using the same temperature regulation system as with exfoliation of graphite in SC. Following exfoliation, the dispersions were transferred to centrifuge tubes where they were allowed to settle overnight. After the settling period, the dispersions were centrifuged using the same centrifuge as in the graphene/SC dispersions (section 3.2.1) for 30 min at 221.21 RPM which corresponds to a RCF of 270 G. The supernatant was then transferred into a new centrifuge tube and centrifuged again for 30 min at 221.21 PRM. All the transfers were done in a manner that did not disturb the sediment at the bottom of the centrifuge tubes. Following centrifugation, a UV-Vis spectrum was recorded to determine the resulting graphene concentration.

3.2.3 Loading of AuNPs onto Graphene Dispersion

A Hydrogen tetrachloroaurate (III) hydrate (49 % Au) precursor was added dropwise to the graphene dispersion so that there would be 1% wt Au loading. Concentrated NH_4OH (32 %) was added dropwise to the graphene/precursor composite to raise the pH to 10.5. The pH was measured using a InLab® Expert NTC 30 pH probe and an inoLab pH7310 pH meter. This solution was then stirred for 25 h under ambient conditions[65].The composite used for the making of the electrodes (section 3.2.1) was then dialyzed for 2 h

under magnetic stirring using the same membranes as previously mentioned. The volume ratio of the sample and the dialysate was 1:300.

3.3 Preparation of Electrodes

3.3.1 Spray-Coating Graphene/AuNPs composite onto Substrates

The graphene/AuNPs composite were manually spray coated onto glass substrates and Sigradur G glassy carbon substrates from HTW Hochtemperatur-Werkstoffe GmbH using a standard airbrush pen. This was done on a hot plate set to around 350 °C. The high temperature aided in the evaporation of water from the composite and lead to a more even spray coating. The substrates were taped to aluminum foil using a heat resistant tape in order to achieve a film with straight edges with an average electrode area of 5.98 cm^2.

3.3.2 Drop-Casting Graphene/AuNPs composite onto Carbon Felt Substrate

A 1.50 cm by 2.00 cm piece of 3.18 mm thick, 99.0 % CF from Alfa Aesar was sonicated in ethanol for 5 min and then sonicated in water for 5 min. The felt was then dried in an oven for 5 min at 85 °C. A carbon rod (99.999 %) from Stream Chemicals, INC. was cut to 10 cm and glued onto the CF using Electrodag PF-407C carbon glue from Acheson. This was allowed to sit overnight to dry in ambient conditions. The following morning the electrode was turned, and 0.5 mL of the composite was drop-cast onto the CF and again allowed to dry overnight in ambient conditions. Three different CF electrodes were prepared: one was just pristine carbon felt; the second was with the graphene/SC dispersion and the third was with the graphene/AuNPs composite. The following day, the carbon rod was wrapped with Teflon tape so that the geometric surface area of the electrode was 3 cm^2.

3.4 Characterization Methods

3.4.1 UV-Vis Analysis

UV-Vis measurements were recorded to determine the concentration of pure graphene in the dispersions. The samples were diluted 251 times to ensure that the absorbance was within the linear range of the instrument. The measurements were recorded using a Shimadzu UV-2501PC spectrophotometer. The spectrum was recorded from 900 nm to 190 nm. The sampling interval was set to 0.5 nm using a fast scan speed with a slit width of 0.5 nm. The graphene concentration (c) was calculated using Beer-Lambert's law. *The* absorbance (A) was recorded at 660 nm to comply with the standard methods found in literature; a cuvette with a path length (b) of 1 cm was used. The extinction coefficient (ε) was determined by Lund et al.[33] to be 6590 $mL \cdot mg^{-1} \cdot m^{-1}$.

3.4.2 Nitrogen Physisorption Analysis

The specific surface area and pore volume of the graphene/SC CF electrode and the graphene/AuNPs CF electrode were measured using nitrogen physisorption. The instrument used was MicroActive 3FlexTM 3500 (Micromeritics). The electrodes were cut into thin strips and degassed for 4 h at 180 °C prior to the analysis. The B.E.T. equation was used to calculate the surface area, whereas the DFT method was used to calculate the pore volume.

3.4.3 ICP-OES Analysis

The gold content of the graphene composite used for the preparation of the electrode and the gold content of the post-electrolysis solution were both analyzed using a Varian Liberty 110 ICP Emission Spectrometer. Argon plasma was used to excite the gold atoms. Prior to the ICP-OES analysis, the graphene composite underwent microwave digestion in sulfuric acid.

3.4.4 TEM Analysis

Microphotographs of the dispersions were obtained using a JEOL JEM 1400 Plus Transmission Electron Microscope operated at 120 kV accelerated voltage and 0.38 nm resolution. The AuNPs particle sizes were analyzed using the ImageJ software. A sample size of 186 particles was used for the graphene composite that was dialyzed before the loading of AuNPs, a sample size of 980 particles was used for the graphene composite that was dialyzed after the loading of the AuNPs and a sample size of 600 particles was used for the graphene composite used in the preparation of electrodes.

3.4.5 SEM and EDS Analysis

The surface morphology of the graphene/AuNPs composite spray coated onto a glass substrate was analyzed using a Leo Gemini 1530 scanning electron microscope with a Thermo Scientific Ultra Dry Silicon Drift Detector. The gold content of the graphene/AuNPs composite that was spray coated onto the glass substrate was analyzed using a Thermo Scientific Apreo S. scanning electron microscope and an Oxford Instruments Ultim Max 100 energy dispersive x-ray spectrometer.

3.4.6 AFM Film Thickness Analysis

The film thickness of the graphene/SC and graphene/AuNPs films applied to a glass substrate were recorded using a NTEGRA PRIMA AFM instrument from NT-MDT, Moscow, Russia. Three different images were recorded for each film. The resulting images were 100 µm by 100 µm (256 pixels by 256 pixels). The measurements were conducted under ambient conditions (RH% = 54.7 and T = 21 ° C) using tapping mode. A HQ:NSC14/AI BS pyramidal silicon cantilever tip with an 8 nm tip radius was used. The resulting images were analyzed using the SPIP™ image analysis software from Image Metrology in Lyngby, Denmark.

3.4.7 4-Probe Conductivity Analysis

The conductivity of the films was measured using a four-probe technique in a linear configuration with a tip spacing of 1.82 mm. A bias current of 1 mA was applied using a Keithley 2400 Sourcemeter. The measurements were taken under ambient conditions (RH% = 45.9 and T = 22.0 °C).

3.4.8 EIS Analysis

The Electrochemical Impedance Spectroscopy (EIS) was measured using a 3-electrode system. Two different WEs were used during this measurement: a GC substrate spray coated with a graphene/SC dispersion and a GC substrate spray coated with a graphene/AuNPs composite. The RE was the same as in the CV experiments. The CE was a carbon rod. Both the WE and CE were physically cleaned by polishing the electrodes with alumina powder (0.3 µm) followed by sonication for 5 min. The measurements were carried out in 0.1 M sodium sulphate solution that had been purged for 15 minutes with N_2 gas. The applied DC potential was 0 V versus the open circuit potential. The AC voltage amplitude used was 10 mV and the frequency ranged from 100 kHz to 0.01 Hz. The measurements were recorded using a Gamry Reference 620 Potentiostat/Galvanostat/ZRA and were recorded using the Gamry Framework version 7.9.0 program. The measurements were analyzed using the Gamry analyst version 7.9.0 program.

3.4.9 CV Analysis

The CV measurements were carried out in an H-Cell from Latech Scientific Supply Pte. Ltd. using a 3- electrode system as shown in (Figure 7). The WE and the RE were on one side of the cell while the CE was on the other. The two cells were separated using a Nafion 117 membrane. The membrane was pre-treated by boiling it in 3% (by volume) H_2O_2 solution for 1 h, rinsed with water and then boiled in 2 M sulfuric acid for 1 h. The WE was either pure carbon felt, graphene/SC dispersion on CF or graphene/AuNPs composite on carbon felt. The RE was Ag/AgCl in a 3.0 M KCl solution. The CE was carbon cloth wrapped around a carbon rod. For all measurements, a 0.1 M NaOH electrolyte solution was used. The glucose concentration used throughout the analysis was either 0.1 M or 5 mM. The solutions were purged with N_2 gas for 15 min prior to starting the measurements. The CV measurements were carried out in an unstirred solution. A potential range of from -0.8 V to 0.8 with a scan rate of 5 $mV \cdot s^{-1}$ was used. All measurements were recorded using an Autolab Frequency Response Analyzer System with the General-Purpose Electrochemical System (GPES) version 4.9.006 software.

Figure 7: Image of the H-Cell set up used for the CV and chronoamperometric measurements.

3.4.10 Chronoamperometry

The chronoamperometric measurements were conducted using the same H-cell setup and potentiostat as in the CV experiments. The cathode solution was 0.1 M NaOH. The anode solution was 0.1 M glucose in 0.1 M NaOH. The solutions were purged with N_2 gas for 15 min prior to the start of the measurement. A potential scan from -0.8 V to 0.8 V with a scan rate of 5 $mV \cdot s^{-1}$ was taken in order to find the potential on the reverse scan where the gold oxide was reduced back to gold and where the oxidation of glucose started. This was found to be at around 0.4 V on the reverse scan and thus a second CV was ran and stopped at around this potential– this was not done on the first chronoamperometric measurement but was carried out for the subsequent measurements. The chronoamperometric measurements were then carried out at 0.159 V for 3 h. Following the electrolysis, an aliquot of the glucose solution was neutralized using 0.5 M H_2SO_4 to ensure that no further reactions would occur in the solution. Throughout the measurements the pH was regularly checked using Whatman indicator paper pH 1.0 – 14.0 full range to check the progress of the reaction.

3.4.11 HPLC Analysis

A 1.0 mL aliquot of the sample collected following the electrolysis and 1.0 mL of water were washed through a 3 mL Supelclean LC-SCX™ SPE tube from Supelco ® and then filtered using a CLARIFY-PVDF 13 mm Syringe Filter in order to remove the sodium ions. The run on 10 µL of the filtered sample was analyzed via HPLC with a refractive index detector. The HPLC column used was an Aminex HPX-87C. The column was held to a constant temperature of 50 °C. The mobile phase used was a 1.2 mM $CaSO_4$ solution

and had a flow rate of 0.3 mL · min^{-1}. A 0.1 M glucose, 0.05 M fructose and 0.02 M gluconic acid solution in 0.1 M NaOH stock solution was prepared for calibration purposes. The solution was then diluted 2 and 5 times in order to construct a calibration curve that were used to analyze the analyte concentration. The stock solution followed the same sample preparation method as the sample.

4 Results and Discussion

4.1 Graphite Exfoliation

4.1.1 Optimization of Graphite/SC Exfoliation and Dialysis Time

The conditions for the graphite/SC exfoliations were first optimized using a 10 mL graphite/SC solution. A thorough examination of how the type of graphite, the rotor speed, the length of the exfoliation, the duration of the dialysis and the number of water changes made throughout the dialysis affected the resulting graphene concentration was conducted. The results of which can be seen in appendix Table A1. From the optimization trials it was determined that the Finnish graphite produced the highest pre-dialysis graphene concentration at 2.91 mg·mL^{-1}. However, the Finnish graphite was not chosen for further experimentation as a commercially available product was used. The graphite from Sigma-Aldrich produced the lowest pre-dialysis graphene concentration at 0.92 mg·mL^{-1} which can be attributed to the low rotor speed. The decision to move forward with the Alfa-Aesar graphite over the Sigma-Aldrich graphite was due to its availability in the lab.

A drastic decrease in graphene concentration occurred during dialysis. To determine when the drop in concentration occurred, the graphene concentration of the Alfa-Aesar trial with an exfoliation time of 2.5 h was measured 2 h into the 19 h dialysis via UV-Vis and determined to be 2.36 mg·mL$^{-1.}$ The graphene concentration 2 h into the 19 h dialysis is lower than the graphene concentration before dialysis (2.78 mg□mL^{-1}) but relatively higher than the graphene concentration after the dialysis (0.45 mg□mL^{-1}). Thus, it was determined that a 2 h dialysis was sufficient.

4.1.2 Exfoliation of Graphite/CNC

The optimization of the parameters for the exfoliation of graphite using SC as stabilizer was previously examined and discussed in the appendix (Section 7) of this work. During the electrochemical characterization of the graphene/SC dispersion, degradation of the films occurred on both the GC substrate and the glass substrate. Thus, due to poor adhesion of the graphene/SC dispersion, graphite was exfoliated using CNC as the stabilizer. The exfoliation of graphite to graphene was attempted using two different CNC solutions – one that underwent hydrolysis in sulfuric acid for 1.5 h and one that underwent hydrolysis in sulfuric acid for 2 h. The exfoliation parameters were based on the work by Lund et al.[66] The length of the hydrolysis in sulfuric acid of the CNC solution, the rotor speed (*N*) in RPM,

the length of exfoliation (*t*) in h and the final graphene concentration of the dispersion in mg·mL^{-1} is shown in Table 1.

Table 1 : Optimization parameters of graphite/CNC. Parameters include the length the CNC underwent hydrolysis by sulfuric acid, rotor speed (*N*) , length of exfoliation (*t*) and the graphene concentration after the dialysis.

Length of sulfuric acid hydrolysis (h)	**Rotor speed; *N* (RPM)**	**Length of exfoliation; *t* (h)**	**Graphene concentration (mg · mL^{-1})**
2.0	22000	3.0	0.26
1.5	22000	3.0	0.011

The graphene dispersion prepared using the CNC that underwent a 2 h sulfuric acid hydrolysis had a final graphene concentration of 0.26 mg·mL^{-1}. The graphene dispersion prepared using the CNC that underwent a 1.5 h sulfuric acid hydrolysis had a final graphene concentration of 0.011 mg·mL^{-1}. The final graphene concentration for both exfoliations using CNC was considerably lower than the graphene concentrations prepared using SC as the stabilizer (2.83 mg·mL^{-1}). It was determined that a higher graphene concentration was of high importance. Thus, rather than changing the graphite exfoliation parameters a different carbon substrate was used. CF as a carbon substrate was investigated as a means to obtain better adhesion of the dispersion.

4.2 Effect of AuNPs Loading Time

The effect of the dialysis on the AuNPs was investigated by loading the AuNPs onto graphene before and after the dialysis of the composite. This was tested using the graphene/AuNPs composite that were exfoliated using 10 mL of the graphite/SC solution. The presence of graphene sheets in the dispersion was first confirmed using TEM (Figure A.1). TEM images were used to qualitatively assess the AuNPs particle distribution in the graphene/AuNPs composites. It was found that the composite containing the AuNPs that were loaded after the dialysis (Figure A.2.a) had more dispersed and smaller AuNPs than the composite where the AuNPs were loaded prior to the dialysis (Figure A.2.b). The latter composite also showed hollowed structures (Figure A.3.a) which in some cases were impregnated with AuNPs (Figure A.3.b) a characteristic not seen in the composites where the AuNPs were loaded after dialysis.

The AuNPs in the graphene/AuNPs composites were then quantitatively analyzed using ImageJ software. In the composite where the AuNPs were loaded after the dialysis the median particle size was 12 nm and

the mean particle size was 13 nm. The composite where the AuNPs were loaded before the dialysis the median particle size was 24 nm and the mean particle size was 26 nm. The particle size distribution for the AuNPs loaded after dialysis is shown in Figure A.4.a and the particle size distribution for the AuNPs loaded before dialysis is shown in Figure A.4.b.

4.3 Physico-Chemical Characterization of Graphene and Graphene/AuNPs Composite

The remainder of the characterizations were carried out using graphene dispersion that was exfoliated using a 30 mL graphite/SC solution maintaining the same ratio of graphite to the volume of solution (1 g per 10 ml solution) as with the smaller volume.

4.3.1 SEM Characterization

The morphology of the films spray coated onto glass substrates was assessed via SEM imaging. By viewing the films from the top, both the graphene/SC dispersion (Figure 8.a) and graphene/AuNPs composite (Figure 8.b) show individual bubbles with dark edges. This is indicative of using a heating pad to aid in the spray coating process. An aerosol of the dispersion is formed through the spray-painting gun and once the droplets meet the heated substrate the droplets dry. The outer edge of the droplets has a tendency to dry more quickly. Thus resulting in a darker color around the edges. By viewing the films from the side both the graphene/SC dispersion(Figure 9.a) and graphene/AuNPs composite (Figure 9.b) show individual sheets of graphene.

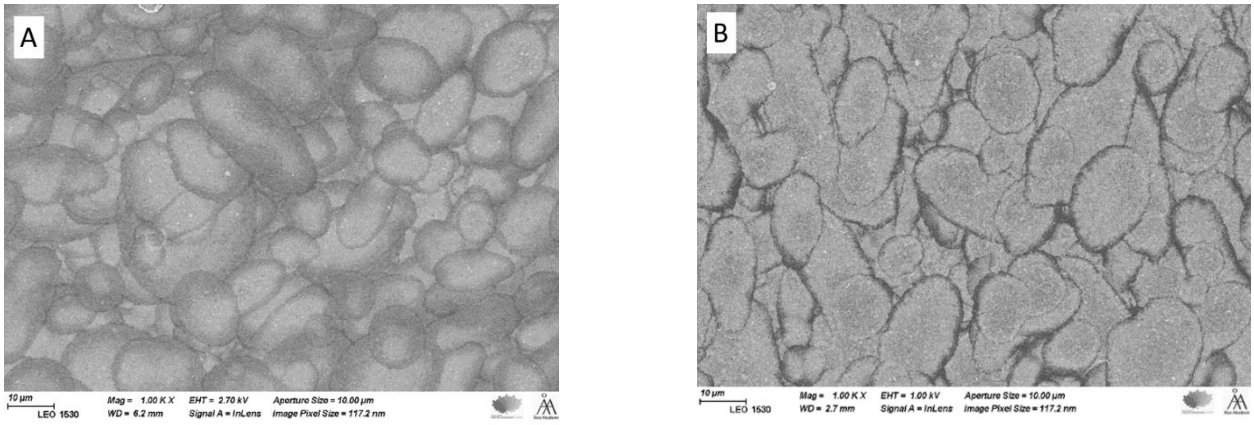

Figure8: SEM image of top view of the (a) graphene/SC carbon on a glass substrate and the (b) graphene/AuNPs on a glass substrate.

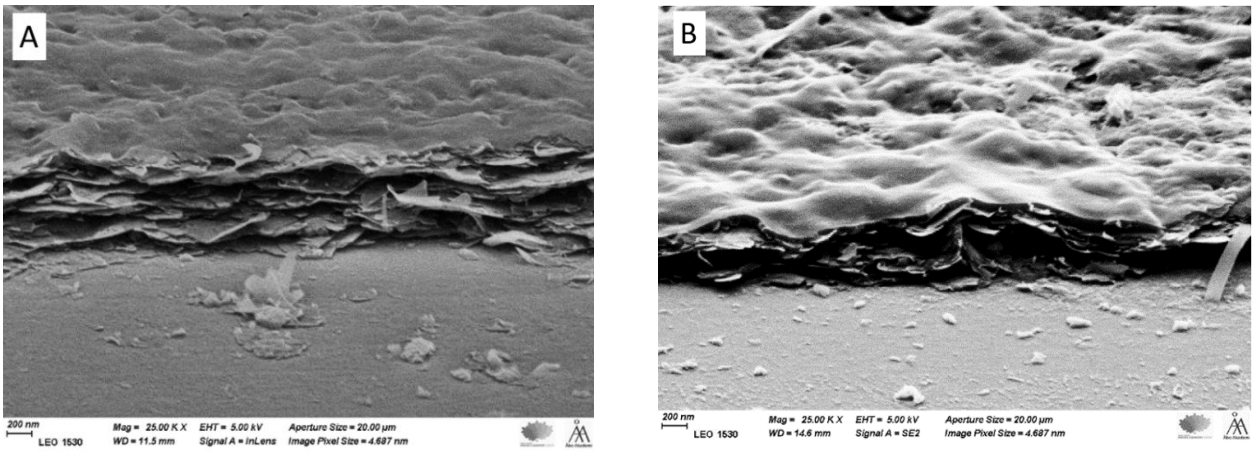

Figure 9: SEM image of side view of the (a) graphene/SC on a glass substrate and the (b) graphene/AuNPs on a glass substrate.

4.3.2 Nitrogen Physisorption

The surface area of the graphene/SC CF electrode and the graphene/AuNPs CF electrode were analyzed via nitrogen physisorption. The BET surface area of the graphene CF electrode was 0.1458 $m^2 \cdot g^{-1}$ and the BET surface area of the graphene/AuNPs CF electrode was 0.1588 $m^2 \cdot g^{-1.}$ These results are expected. The addition of the AuNPs would increase the overall surface area of the electrode without diminishing the graphene.

4.3.3 Au Content Determination by EDS and ICP-OES

The gold content of the graphene/AuNPs composite was analyzed via ICP-OES and determined to be 0.028 ± 0.001 $mg \cdot L^{-1}$ which is shown in Table 2. This was determined to be 0.92 % (w/w) of the graphene/AuNPs composite which was close to our target loading of 1 %. The gold content of the graphene/AuNPs film spray coated onto the GC electrode was analyzed via SEM-EDS and determined to be 0.19 ± 0.04 % (w/w). The lower content measured by EDS on the spray coated film could be indicative to either one of two things: the first is that some gold was lost during the adhesion to the substrate or the second that gold is intercalating between the graphene sheets and not all the gold was characterized. These are both plausible explanations as the gold content in the film is less than the gold content in the composite. However, the first one assumes that the EDS was able to penetrate the entire depth of the film and is a direct representation of the bulk sample. It is more probable that the difference in gold content between the film and the composite is a combination of both.

Table 2: The gold content of the graphene/AuNPs composite as determined by ICP-OES and the gold content of the graphene/AuNPs film spray coated on a glassy carbon electrode as determined by SEM-EDS.

	Analysis method	Gold Content
Graphene/AuNPs composite	ICP-OES	0.028 ± 0.001 mg · mL^{-1}
Graphene/AuNPs on Glassy Carbon Electrode	EDS	0.19 ± 0.04 % (w/w)

4.3.4 TEM Characterization

As a dispersion with a higher initial volume of graphite/SC solution was used, TEM images were again recorded to confirm the presence of graphene sheets. As seen in Figure 10, the exfoliation of graphite did lead to graphene as there are distinct graphene sheets throughout the image.

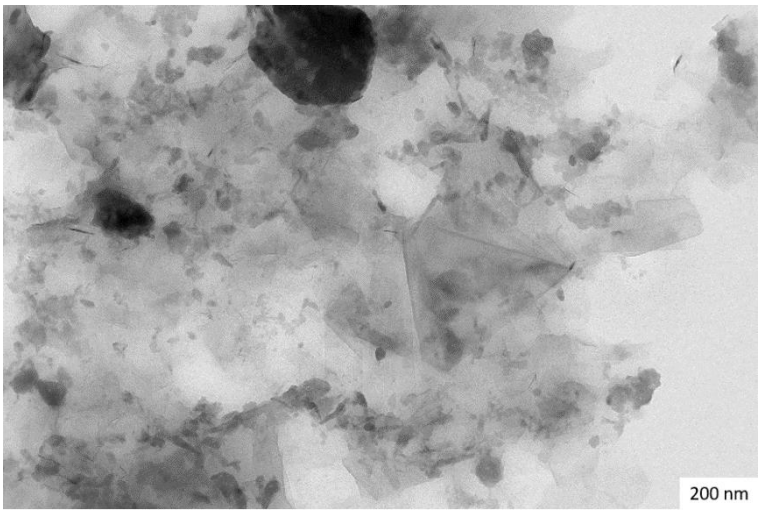

Figure 10: TEM image of graphene/SC dispersion that was used for AuNPs loading.

TEM images were used to quantify the particle sizes of the AuNPs as well as qualitatively assess the particle distribution of the graphene/AuNPs composite. The AuNPs particle size in the graphene/AuNPs composite was analyzed using ImageJ software. The image (Figure 11) shows both the AuNPs and the sodium ions resulting from the surfactant. The sodium ions are referenced by the pink arrow in Figure 11 and were not counted towards the AuNPs particle size distribution (Figure 12). Based on the images from Figure 11, it can be concluded that the AuNPs were well dispersed throughout the graphene/AuNPs composite and had both a mean and medium diameter of 13 nm; thus corroborating with the average particle size resulting from the optimization trials in section 4.2.

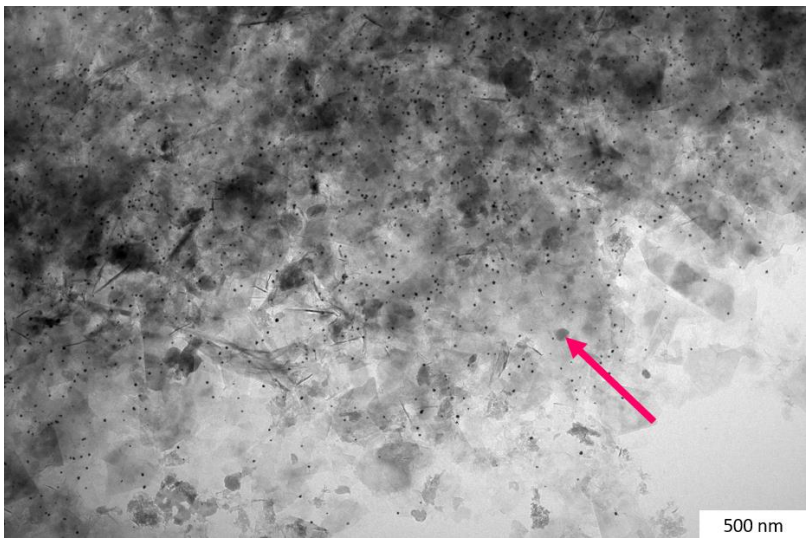

Figure 11: TEM image of graphene/AuNPs composite that was used for drop-casting onto carbon felt electrode.

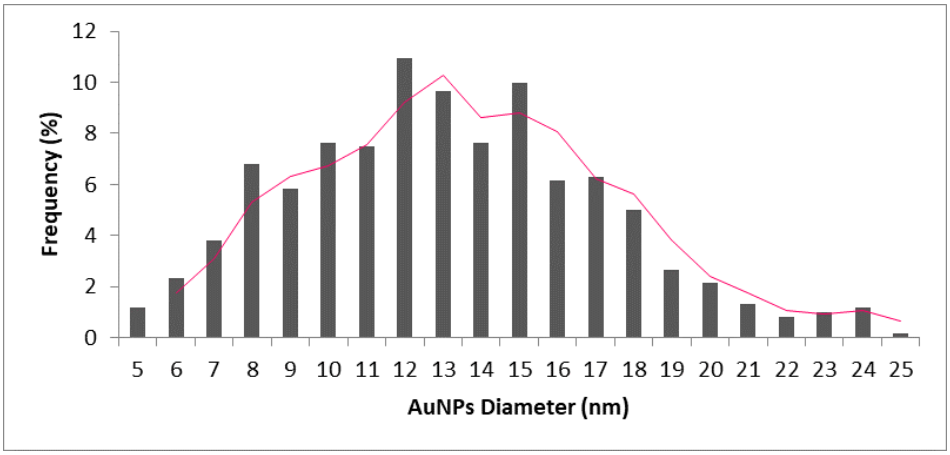

Figure 12: Density distribution of AuNPs loaded onto graphene composite used for drop-casting onto carbon felt.

4.4 Electrochemical Characterization

4.4.1 Conductivity of Films

The conductivity of the graphene/SC and the graphene/AuNPs films on a glassy substrate were calculated using the 4PP and determined to be $6.3 \cdot 10^2$ $S \cdot m^{-1}$ and $1.3 \cdot 10^3$ $S \cdot m^{-1}$ respectively. The conductivity of the graphene/SC (2.83 $mg \cdot mL^{-1}$) is considerably lower than that in literature which was recorded to be $1.7 \cdot 10^4$ $S \cdot m^{-1}$ when the resulting graphene/SC concentration was 3 $mg \cdot mL^{-1}$. [33] The lower conductivity in this work could be attributed to the difference in dialysis procedures. The composite in this work was dialyzed twice and the one in literature was dialyzed once. Table 3 shows the film type, the volume of the dispersion used per film (mL), the average film thickness as determined by AFM (µm), the film area (cm^2) and the resulting conductivity ($S \cdot m^{-1}$).

Table 3: The film type, the volume of the dispersion per film, the average film thickness, the area of the film and the resulting conductivity.

Film	Vol. Of Dispersion (mL)	Average Film Thickness (μm)	Film Area (cm^2)	Conductivity ($S \cdot m^{-1}$)
Graphene/SC	2.5	1.9 ± 0.46	5.6	$6.3 \cdot 10^2$
Graphene/AuNPs	2.5	0.92 ± 0.27	5.4	$1.3 \cdot 10^3$

The average height of the graphene/AuNPs film as determined by AFM was 0.92 ± 0.27 μm while the average height of the graphene/SC film as determined by AFM was 1.9 ± 0.46 μm. These numbers slightly differ from the SEM thickness which were determined to be 0.63 μm and 2.2 μm respectively. While the films were prepared in the same manner, the difference in film thickness could be attributed to the fact that the measurements were not taken on the same film and the slight difference in the spray coating process among different films. The thickness of the film as determined by AFM provides a more accurate representation of the films as with AFM multiple measurements were taken over three different areas and then averaged. Whereas the SEM thickness values are only recorded at one specific region.

4.4.2 EIS of Graphene/AuNPs on GC Electrode

EIS of a pristine GC electrode and a GC electrode spray coated with 5 mL of the graphene/AuNPs composite was carried out in a 0.1 M sodium sulphate solution with a frequency range from 100 kHz to 0.01 Hz. The use of the GC electrode in the electrochemical methods allowed for minimal electrode preparations prior to the start of the analysis. Figure 13 shows the impedance spectrum of both the pristine GC electrode (orange) and the GC electrode spray coated with the graphene/AuNPs composite (blue). The pristine GC electrode has a higher resistance as indicated by the higher imaginary impendence value. The low frequency capacitance for the pristine GC electrode is 2.70 μF and for the GC electrode that was spray coated with the graphene/AuNPs the low frequency capacitance is 7.30 μF. Thus, indicating that the composite increased the overall capacitance of the electrode. This is expected as the composite would increase the overall surface area of the electrode and as surface area increases so to does the capacitance.

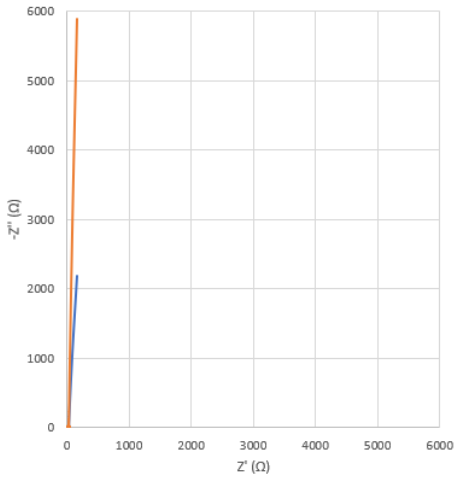

Figure 13 : EIS spectra of pristine glassy carbon electrode (orange) and graphene/AuNPs composite spray coated on glassy carbon electrode (blue) in 0.1 M sodium sulphate solution.

4.4.3 Cyclic Voltammetry of electrodes

4.4.3.1 Glassy Carbon Substrate

The cyclic voltammetry (CV) experiments that used GC as the substrate were carried out in two different cell configurations: an H-Cell (shown in section 3.4.8) and a small-cell configuration (Figure 14). The small-cell configuration was examined as a way to mitigate the degradation of the graphene/AuNPs film on the GC electrode. It was hypothesized that with the small-cell setup there would be a smaller volume of solution interacting with the film which would minimize the degradation. However, degradation of the film occurred over the entire area that was covered by the solution. The degradation of the films on the GC substrate could be attribute to the surface characteristics of the support as it is both smooth and hydrophobic.[17]

Figure 14: The small-scale configuration used to conduct the CV on the glassy carbon electrodes.

The cyclic voltammograms shown in Figure 15 were recorded using the H-cell configuration in 0.1 M NaOH with a scan rate of 10 mV·s^{-1} using a pristine GC electrode (Figure 15.a) and a GC electrode spray coated with the graphene/AuNPs composite (Figure 15.b). In the CV of the pristine GC electrode there are no clear indications of an electrochemical process taking place.[17] It can also be seen that the current of the pristine GC electrode is much smaller than that with the graphene/AuNPs composite – the GC electrode's max current is around 0.7 mA whereas the max current for the electrode with graphene/AuNPs electrode is around 7.0 mA. In Figure 15.b a shoulder appears in the anodic scan at ~0.5 V. This shoulder is indicative to the oxidation of gold at the electrode surface[28], which is absent in the pristine GC electrode. This peak is drastically decreased between the first (pink) and tenth scan (black). This decrease could be attributed to the degradation of the film.

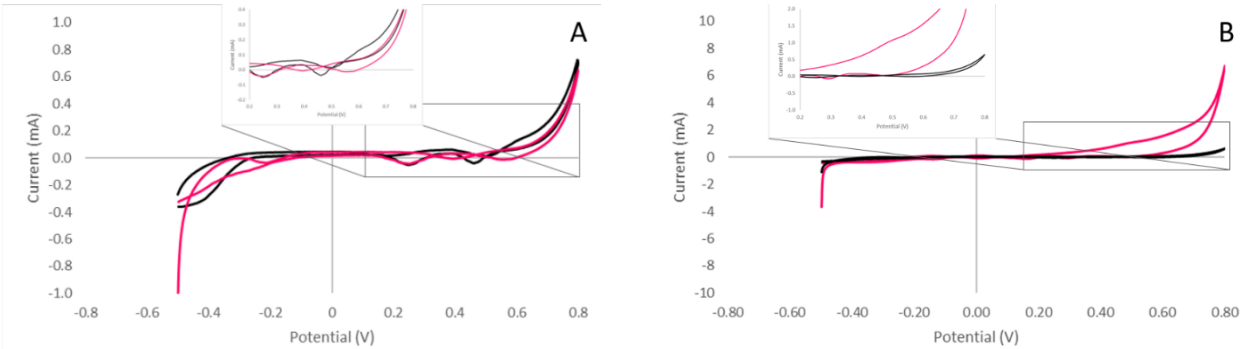

Figure 15 : CV of the 1st scan (pink) and 10th scan (black) of the (a) pristine GC electrode and the (b) GC electrode spray coated with the graphene/AuNPs composite. Both were recorded in a 0.1 M NaOH solution with a scan rate of 10 mV · s^{-1} with a potential range of -0.8 V to 0.8 V.

The CV shown in Figure 16 was recorded using the small-cell configuration with a scan rate of 10 mV·s $^{-1}$ with a GC electrode spray coated with the graphene/AuNPs composite in a 0.1 M glucose in 0.1 M NaOH solution. The electrochemical reactions associated with glucose were confirmed (Figure 16) by the sharp peak at ~ 0.2 V in the reverse scan which indicate the oxidation of glucose. [17,28]

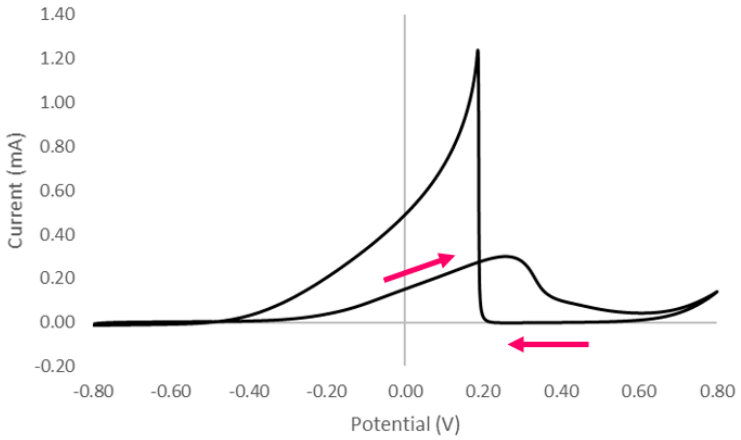

Figure 16 : CV of the GC electrode spray coated with the graphene/AuNPs composite in a 0.1 M glucose in 0.1 M NaOH solution recorded in 0.1 M NaOH solution with a scan rate of 10 mV · s^{-1} with a potential range of -0.8 V to 0.8 V in the small-scale configuration.

However, degradation of the film still occurred at the solution interface. It was determined that the film degradation was not dependent on the cell configuration but was due in part to the adhesion of the composite to the carbon substrate. Moving forward, glucose ECO on graphene/AuNPs was carried out using a carbon felt (CF) substrate in an H-cell configuration.

4.4.3.2 Carbon felt Substrate

The CV of the graphene/AuNPs CF electrode in a 5 mM glucose in 0.1 M NaOH solution with a scan rate of 1 mV·s^{-1} is shown in Figure 17. A lower glucose concentration was used to control the maximum current – as a larger glucose concentration would result in a higher peak and complicate the evaluation of the peak. A lower scan rate was used in order to minimize the effects of the capacitive current and ensure that the CV was a result of the Faradaic current.[67]

In the forward (anodic) scan, the peaks at both ~0.15 V and ~0.30 V can be attributed to the oxidation of glucose. According to literature, the peak at ~0.15 V is due to the dehydrogenation of the anomeric carbon on glucose molecule.[6,68] The glucose molecule is further oxidized to gluconolactone.[68] The peak at ~0.30 V is due to the oxidative production of gluconate. The peak at ~ 0.5 V is due to oxidation of the AuNPs on the electrode.[17,28] During the reverse (cathodic) scan, the oxidized gold species are reduced.

This generates fresh gold surfaces allowing for the oxidation of glucose to occur at ~0.16 V.[6,17,68] The peak at ~ -0.39 V could be attributed to the desorption of the adsorbed species from the electrode surface.

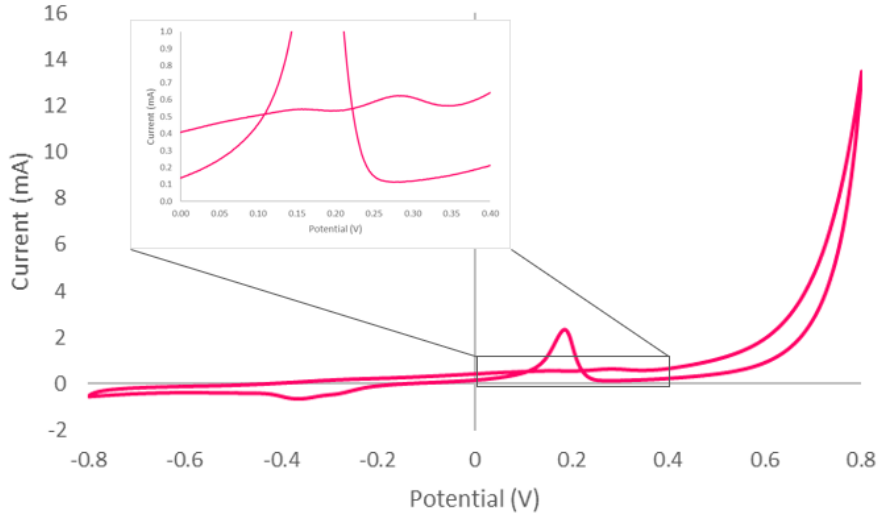

Figure 17: The cyclic voltammogram of the graphene/AuNPs electrode in a 5 mM glucose in 0.1 M NaOH solution with a scan rate of 1 mV · s^{-1}.

The CV (Figure 18) of a 5 mM glucose solution in 0.1 M NaOH with a scan rate of 5 mV·s^{-1} was carried out using a pristine CF electrode (black), a CF electrode drop casted with a graphene/SC dispersion (purple) and a CF electrode drop casted with a graphene/AuNPs composite (pink). It was determined that the glucose oxidation occurred at 0.16 V in the reverse scan using the graphene/AuNPs CF electrode. This peak was absent for the scans using both the pristine CF electrode and the graphene/SC CF electrode and corresponds to those found in literature[28]. Thus, confirming that the glucose oxidation occurs in the presence of the AuNPs which act as a catalyst for the glucose electrocatalytic oxidation (ECO).

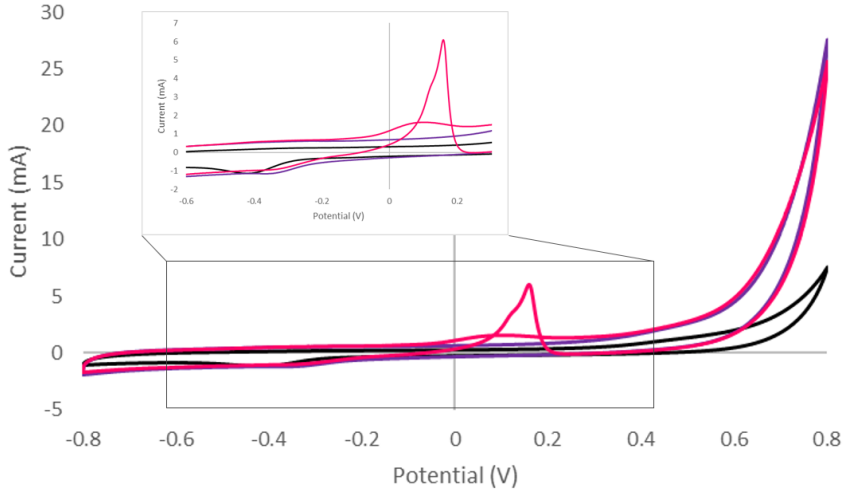

Figure 18: The cyclic voltammogram of the pristine carbon felt electrode (black), graphene/SC electrode (purple) and graphene/AuNPs electrode (pink) in a 5 mM glucose in 0.1 M NaOH solution with a scan rate of 5 mV · s^{-1}.

As the peak formed at ~0.16 V in the reverse scan corresponds to glucose oxidation, the relationship between its peak intensity and the scan rate was investigated. A linear relationship between the scan rate and the current intensity is indicative of a surface reaction process while a linear relationship between the square root of the scan rate and current intensity is indicative of a diffusion-controlled process.[69] The glucose oxidation peak at ~0.16 V shows no linearity to either the scan rate (Figure 19.a) nor the square root of the scan rate (Figure 19.b). This indicates that there is both a surface reaction process and a diffusion-controlled process taking place at the electrode. [69]

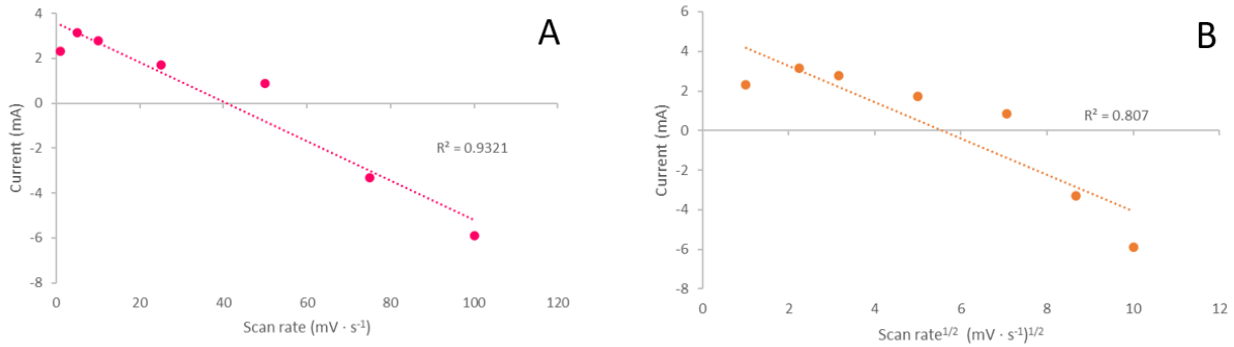

Figure 19: The relationship between the a) scan rate (V · s^{-1}) and the current and the b) square root of the scan rate and the current of the glucose oxidation peak on the graphene/AuNPs electrode.

4.5 Electrocatalytic Oxidation of Glucose on Graphene/AuNPs Catalyst

4.5.1 Chronoamperometric Measurements

The electrolysis of glucose to gluconic acid was conducted using chronoamperometry at an applied potential of 0.16 V in an H-cell configuration with a 0.1 M glucose in 0.1 M NaOH solution that was under magnetic stirring. The applied potential was determined by CV in section 3.4.3 as the point in which glucose oxidation occurs. The chronoamperometric measurements in Figure 20 show a higher current density for the graphene/AuNPs electrode versus the pristine CF and graphene/SC CF electrode. This suggests that the electrolysis of glucose to gluonic acid occurs only on the graphene/AuNPs electrode. The decrease in current density of the graphene/AuNPs electrode can be attributed to the surface poisoning of the electrode by the adsorption of gluconic acid and/or its analogues.[6,23,26]

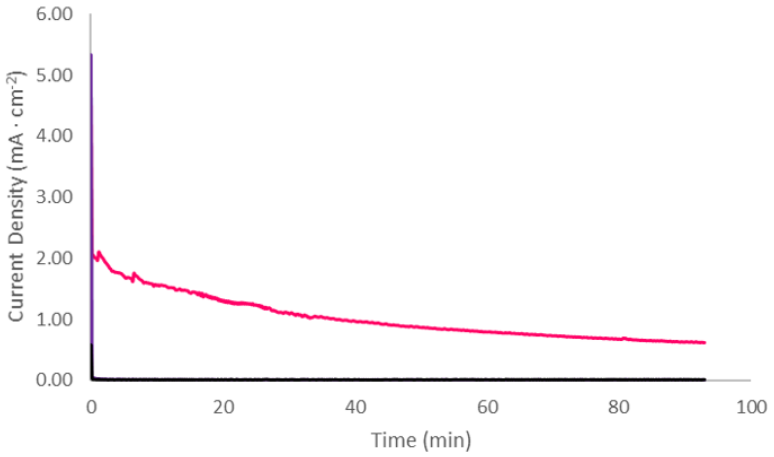

Figure 20: Chronoamperogram of the electrolysis of glucose into gluconic acid using a graphene/AuNPs carbon felt electrode (pink), a graphene/SC carbon felt electrode (purple) and a pristine carbon felt electrode (black) ran in 0.1 M glucose in 0.1 M NaOH solution for 3 hours with an applied potential of 0.159 V.

Following 3 h of electrolysis, 17.57 mM of gluconic acid was produced using the graphene/AuNPs electrode. No gluconic acid was produced using the graphene/SC CF electrode nor the pristine CF electrode. Confirming the production of gluconic acid can be attributed to the presence of the AuNPs which act as the catalyst for the glucose ECO.

4.5.2 Activity and Stability of Electrode

To evaluate the glucose ECO activity and stability, repeated electrolysis experiments were carried out over multiple days using the same graphene/AuNPs electrode. Figure 21 shows the chronoamperogram obtained for the electrolysis of glucose to gluconic acid that was ran on different days. The data shows that the obtained current density decreased after each electrolysis experiment, indicating the deactivation of the catalyst.

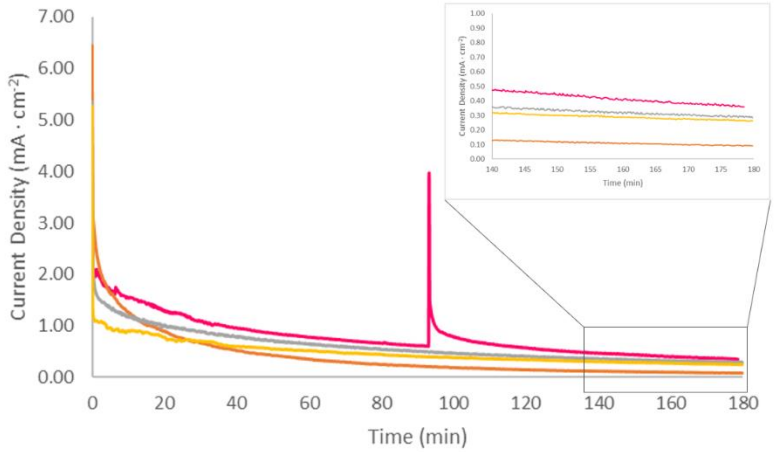

Figure 21: Chronoamperogram of the electrolysis of glucose into gluconic acid using a graphene/AuNPs carbon felt electrode for the first time (pink), on the second day (orange), on the third day (grey) and the fourth day (yellow) ran in 0.1 M glucose in 0.1 M NaOH solution for 3 h with an applied potential of 0.159 V.

Graphene/AuNPs were observed to be very active towards glucose ECO. The average TOF after 3 h for the four electrolysis was $1.97 \cdot 10^3$ h^{-1} which corresponds to an average glucose conversion of 18 % (Table 4). The gold content in the electrolysis solution taken at the end of the 3 h experiment was analysis by ICP-OES and determined to be below the limit of detection for the instrument. Concluding that the gold metal did not leach into the solution.

Table 4: a comparison of the concentration of gluconic acid (mM), the glucose conversion (%), the TOF (h^{-1}) of the electrolysis of glucose to gluconic acid ran in a 0.1 M glucose in 0.1 M NaOH solution for 3 hours with an applied potential of 0.159 V over multiple days.

	Concentration of Gluconic Acid (mM)	**Glucose Conversion (%)**	**TOF (h^{-1})**
First Electrolysis	17.57	19	$2.06 \cdot 10^3$
Second Electrolysis	17.08	19	$2.00 \cdot 10^3$
Third Electrolysis	16.72	18	$1.96 \cdot 10^3$
Fourth Electrolysis	15.93	17	$1.87 \cdot 10^3$

5 Conclusions

The aim of this study was to prepare and characterize a graphene/AuNPs composite to be used as an electrocatalyst for the conversion of glucose into gluconic acid and to assess the stability and activity of the catalyst. The graphene dispersion was shear force exfoliated from graphite and the optimal mixing time, rotor speed and dialysis length were determined. The AuNPs were then loaded onto the graphene at a target loading of 1 % wt. and an actual loading of 0.92 % -as determined by ICP-OES.

This composite was then applied to two different carbonous substrate materials, GC and CF. The adhesion of the graphene/AuNPs onto the GC substrate proved to be difficult and resulted in the degradation of the films. The adhesion of the graphene/AuNPs onto the CF proved to be successful. This was determined by the fact that the gold content at the end of the extended electrolysis was below the limit of detection for the ICP-OES instrument.

The physical characteristics of the composites were determined via TEM, SEM and AFM. From these microscopy techniques, it was determined that the graphite exfoliations did produce graphene sheets and that the average particle size of the AuNPs was 13 nm. The electrochemical characterizations proved the oxidation of glucose occurred only on the AuNPs as well as the capacitive behaviour of the graphene/AuNPs composite. The conversion of glucose to gluconic acid following a 3 h electrolysis was confirmed via HPLC.

The activity of the AuNPs catalyst was determined by its TOF. The TOF was determined to be $2.06 \cdot 10^{3}$ h^{-1} which indicated strong activity. By analyzing the change in the TOF, the resulting chronoamperogram and the final gluconic acid production after four 3 h electrolysis; the electrode and catalyst was determined to be stable.

Further perspectives in to this field could include the determination of the reaction mechanism at the gold surface. An investigation of the degradation of the films on GC and the use of different substrate materials. Further optimization of the AuNPs loading process to reach a higher amount and an optimal AuNPs size could also be investigated as a way to increase the overall production of gluconic acid.

6 References

(1) Sun, Y.; Cheng, J. Hydrolysis of Lignocellulosic Materials for Ethanol Production: A Review. *Bioresour. Technol.* **2002**, *83* (1), 1–11. https://doi.org/10.1016/S0960-8524(01)00212-7.

(2) Muscat, A.; de Olde, E. M.; de Boer, I. J. M.; Ripoll-Bosch, R. The Battle for Biomass: A Systematic Review of Food-Feed-Fuel Competition. *Glob. Food Secur.* **2020**, *25*, 100330. https://doi.org/10.1016/j.gfs.2019.100330.

(3) Pletcher, D.; Greef, R.; Peat, R.; Peter, L. M.; Robinson, J. *Instrumental Methods in Electrochemistry*, Repr.; Ellis Horwood series in physical chemistry; Horwood: Chichester, 2011.

(4) McQuarrie, D. A.; Simon, J. D. *Physical Chemistry: A Molecular Approach*; University Science Books: Sausalito, Calif, 1997.

(5) Frontana-Uribe, B. A.; Little, R. D.; Ibanez, J. G.; Palma, A.; Vasquez-Medrano, R. Organic Electrosynthesis: A Promising Green Methodology in Organic Chemistry. *Green Chem.* **2010**, *12* (12), 2099. https://doi.org/10.1039/c0gc00382d.

(6) Moggia, G.; Kenis, T.; Daems, N.; Breugelmans, T. Electrochemical Oxidation of D -Glucose in Alkaline Medium: Impact of Oxidation Potential and Chemical Side Reactions on the Selectivity to D -Gluconic and D -Glucaric Acid. *ChemElectroChem* **2020**, *7* (1), 86–95. https://doi.org/10.1002/celc.201901592.

(7) Vassilyev, Yu. B.; Khazova, O. A.; Nikolaeva, N. N. Kinetics and Mechanism of Glucose Electrooxidation on Different Electrode-Catalysts. *J. Electroanal. Chem. Interfacial Electrochem.* **1985**, *196* (1), 127–144. https://doi.org/10.1016/0022-0728(85)85085-3.

(8) Hustede, H.; Haberstroh, H.-J.; Schinzig, E. Gluconic Acid. In *Ullmann's Encyclopedia of Industrial Chemistry*; Wiley-VCH Verlag GmbH & Co. KGaA, Ed.; Wiley-VCH Verlag GmbH & Co. KGaA: Weinheim, Germany, 2000; p a12_449. https://doi.org/10.1002/14356007.a12_449.

(9) Paton, K. R.; Varrla, E.; Backes, C.; Smith, R. J.; Khan, U.; O'Neill, A.; Boland, C.; Lotya, M.; Istrate, O. M.; King, P.; Higgins, T.; Barwich, S.; May, P.; Puczkarski, P.; Ahmed, I.; Moebius, M.; Pettersson, H.; Long, E.; Coelho, J.; O'Brien, S. E.; McGuire, E. K.; Sanchez, B. M.; Duesberg, G. S.; McEvoy, N.; Pennycook, T. J.; Downing, C.; Crossley, A.; Nicolosi, V.; Coleman, J. N. Scalable Production of Large Quantities of Defect-Free Few-Layer Graphene by Shear Exfoliation in Liquids. *Nat. Mater.* **2014**, *13* (6), 624–630. https://doi.org/10.1038/nmat3944.

(10) Lam, E.; Luong, J. H. T. Carbon Materials as Catalyst Supports and Catalysts in the Transformation of Biomass to Fuels and Chemicals. *ACS Catal.* **2014**, *4* (10), 3393–3410. https://doi.org/10.1021/cs5008393.

(11) Delidovich, I. V.; Taran, O. P.; Matvienko, L. G.; Simonov, A. N.; Simakova, I. L.; Bobrovskaya, A. N.; Parmon, V. N. Selective Oxidation of Glucose Over Carbon-Supported Pd and Pt Catalysts. *Catal. Lett.* **2010**, *140* (1–2), 14–21. https://doi.org/10.1007/s10562-010-0430-0.

(12) Taube, M. *Storange and Transmission of Secondary Energy*; 377; Eidg. Institut fur Reaktorforschung: Wurenlingen Schweiz, 1979.

(13) Energy Information Administration. Petroleum Supply Monthly. *May 2022*, 1.

(14) Lucas, F. W. S.; Grim, R. G.; Tacey, S. A.; Downes, C. A.; Hasse, J.; Roman, A. M.; Farberow, C. A.; Schaidle, J. A.; Holewinski, A. Electrochemical Routes for the Valorization of Biomass-Derived Feedstocks: From Chemistry to Application. *ACS Energy Lett.* **2021**, 1205–1270. https://doi.org/10.1021/acsenergylett.0c02692.

(15) Isikgor, F. H.; Becer, C. R. Lignocellulosic Biomass: A Sustainable Platform for the Production of Bio-Based Chemicals and Polymers. *Polym. Chem.* **2015**, *6* (25), 4497–4559. https://doi.org/10.1039/C5PY00263J.

(16) Sturgeon, R. J. Monosaccharides. In *Methods in Plant Biochemistry*; Elsevier, 1990; Vol. 2, pp 1–37. https://doi.org/10.1016/B978-0-12-461012-5.50007-0.

(17) Pasta, M.; Ruffo, R.; Falletta, E.; Mari, C. M.; Pina, C. D. Alkaline Glucose Oxidation on Nanostructured Gold Electrodes. *Gold Bull.* **2010**, *43* (1), 57–64. https://doi.org/10.1007/BF03214967.
(18) Werpy, T.; Petersen, G. *Top Value-added Chemicals from Biomass: Volume I -- Results of Screening for Potential Candidates from Sugars and Synthesis Gas*; DOE/GO-102004-1992, 15008859; 2004; p DOE/GO-102004-1992, 15008859. https://doi.org/10.2172/15008859.
(19) Rafaïdeen, T.; Baranton, S.; Coutanceau, C. Highly Efficient and Selective Electrooxidation of Glucose and Xylose in Alkaline Medium at Carbon Supported Alloyed PdAu Nanocatalysts. *Appl. Catal. B Environ.* **2019**, *243*, 641–656. https://doi.org/10.1016/j.apcatb.2018.11.006.
(20) Bao, J.; Furumoto, K.; Fukunaga, K.; Nakao, K. A Kinetic Study on Air Oxidation of Glucose Catalyzed by Immobilized Glucose Oxidase for Production of Calcium Gluconate. *Biochem. Eng. J.* **2001**, *8* (2), 91–102. https://doi.org/10.1016/S1369-703X(00)00140-6.
(21) Ibl, N. Nomenclature for Transport Phenomena in Electrolytic Systems. *Pure Appl. Chem.* **1981**, *53* (10), 1827–1840. https://doi.org/10.1351/pac198153101827.
(22) Holade, Y.; Servat, K.; Napporn, T. W.; Morais, C.; Berjeaud, J.-M.; Kokoh, K. B. Highly Selective Oxidation of Carbohydrates in an Efficient Electrochemical Energy Converter: Cogenerating Organic Electrosynthesis. *ChemSusChem* **2016**, *9* (3), 252–263. https://doi.org/10.1002/cssc.201501593.
(23) Tominaga, M.; Nagashima, M.; Nishiyama, K.; Taniguchi, I. Surface Poisoning during Electrocatalytic Monosaccharide Oxidation Reactions at Gold Electrodes in Alkaline Medium. *Electrochem. Commun.* **2007**, *9* (8), 1892–1898. https://doi.org/10.1016/j.elecom.2007.04.024.
(24) Lu, Y.-H.; Zhou, M.; Zhang, C.; Feng, Y.-P. Metal-Embedded Graphene: A Possible Catalyst with High Activity. *J. Phys. Chem. C* **2009**, *113* (47), 20156–20160. https://doi.org/10.1021/jp908829m.
(25) Climent, M. J.; Corma, A.; Iborra, S. Converting Carbohydrates to Bulk Chemicals and Fine Chemicals over Heterogeneous Catalysts. *Green Chem.* **2011**, *13* (3), 520. https://doi.org/10.1039/c0gc00639d.
(26) Tominaga, M.; Shimazoe, T.; Nagashima, M.; Taniguchi, I. Electrocatalytic Oxidation of Glucose at Gold Nanoparticle-Modified Carbon Electrodes in Alkaline and Neutral Solutions. *Electrochem. Commun.* **2005**, *7* (2), 189–193. https://doi.org/10.1016/j.elecom.2004.12.006.
(27) Hassler, M. Other Commonly Used Biomedical Coatings: Pyrolytic Carbon Coatings. In *Coatings for Biomedical Applications*; Elsevier, 2012; pp 75–105. https://doi.org/10.1533/9780857093677.1.75.
(28) Wu, J.-W.; Wang, C.-H.; Wang, Y.-C.; Chang, J.-K. Ionic-Liquid-Enhanced Glucose Sensing Ability of Non-Enzymatic Au/Graphene Electrodes Fabricated Using Supercritical CO2 Fluid. *Biosens. Bioelectron.* **2013**, *46*, 30–36. https://doi.org/10.1016/j.bios.2013.02.021.
(29) Khalil, I.; Julkapli, N.; Yehye, W.; Basirun, W.; Bhargava, S. Graphene–Gold Nanoparticles Hybrid—Synthesis, Functionalization, and Application in a Electrochemical and Surface-Enhanced Raman Scattering Biosensor. *Materials* **2016**, *9* (6), 406. https://doi.org/10.3390/ma9060406.
(30) Solomons, T. W. G.; Fryhle, C. B.; Snyder, S. A. *Organic Chemistry*, 11th edition.; Wiley: Hoboken, NJ, 2013.
(31) Wulfsberg, G. *Foundations of Inorganic Chemistry*; University Science Books: Mill Valley, California, 2018.
(32) Novoselov, K. S.; Geim, A. K.; Morozov, S. V.; Jiang, D.; Zhang, Y.; Dubonos, S. V.; Grigorieva, I. V.; Firsov, A. A. Electric Field Effect in Atomically Thin Carbon Films. *Science* **2004**, *306* (5696), 666–669. https://doi.org/10.1126/science.1102896.
(33) Lund, S.; Kauppila, J.; Sirkiä, S.; Palosaari, J.; Eklund, O.; Latonen, R.-M.; Smått, J.-H.; Peltonen, J.; Lindfors, T. Fast High-Shear Exfoliation of Natural Flake Graphite with Temperature Control and High Yield, 2021.

(34) Zhao, W.; Fang, M.; Wu, F.; Wu, H.; Wang, L.; Chen, G. Preparation of Graphene by Exfoliation of Graphite Using Wet Ball Milling. *J. Mater. Chem.* **2010**, *20* (28), 5817. https://doi.org/10.1039/c0jm01354d.
(35) Taylor, A. C. Advances in Nanoparticle Reinforcement in Structural Adhesives. In *Advances in Structural Adhesive Bonding*; Elsevier, 2010; pp 151–182. https://doi.org/10.1533/9781845698058.1.151.
(36) Hernandez, Y.; Nicolosi, V.; Lotya, M.; Blighe, F. M.; Sun, Z.; De, S.; McGovern, I. T.; Holland, B.; Byrne, M.; Gun'Ko, Y. K.; Boland, J. J.; Niraj, P.; Duesberg, G.; Krishnamurthy, S.; Goodhue, R.; Hutchison, J.; Scardaci, V.; Ferrari, A. C.; Coleman, J. N. High-Yield Production of Graphene by Liquid-Phase Exfoliation of Graphite. *Nat. Nanotechnol.* **2008**, *3* (9), 563–568. https://doi.org/10.1038/nnano.2008.215.
(37) Lotya, M.; King, P. J.; Khan, U.; De, S.; Coleman, J. N. High-Concentration, Surfactant-Stabilized Graphene Dispersions. *ACS Nano* **2010**, *4* (6), 3155–3162. https://doi.org/10.1021/nn1005304.
(38) John, T. P.; Panesar, J. S.; Kowalski, A.; Rodgers, T. L.; P. Fonte, C. Linking Power and Flow in Rotor-Stator Mixers. *Chem. Eng. Sci.* **2019**, *207*, 504–515. https://doi.org/10.1016/j.ces.2019.06.039.
(39) Utomo, A.; Baker, M.; Pacek, A. W. The Effect of Stator Geometry on the Flow Pattern and Energy Dissipation Rate in a Rotor–Stator Mixer. *Chem. Eng. Res. Des.* **2009**, *87* (4), 533–542. https://doi.org/10.1016/j.cherd.2008.12.011.
(40) Nakama, Y. Surfactants. In *Cosmetic Science and Technology*; Elsevier, 2017; pp 231–244. https://doi.org/10.1016/B978-0-12-802005-0.00015-X.
(41) Sirkiä, S. The Optimal Parameters for the Dialysis of Graphene Dispersion, 2018.
(42) Skoog, D. A.; West, D. M.; Holler, F. J. *Fundamentals of Analytical Chemistry*, 7th ed.; Saunders golden sunburst series; Saunders College Pub: Fort Worth, 1996.
(43) Skoog, D. A.; Holler, F. J.; Crouch, S. R. *Principles of Instrumental Analysis*, 7. edition.; Cengage Learning: Boston, MA, 2018.
(44) Ubi, G. M.; Ikpeme, E. V.; Essien, I. S. Essentials of the COVID-19 Coronavirus. In *Data Science for COVID-19*; Elsevier, 2022; pp 1–25. https://doi.org/10.1016/B978-0-323-90769-9.00020-7.
(45) Dollimore, D.; Spooner, P.; Turner, A. The Bet Method of Analysis of Gas Adsorption Data and Its Relevance to the Calculation of Surface Areas. *Surf. Technol.* **1976**, *4* (2), 121–160. https://doi.org/10.1016/0376-4583(76)90024-8.
(46) Bertier, P.; Schweinar, K.; Stanjek, H.; Ghanizadeh, A.; Clarkson, C. R.; Busch, A.; Kampman, N.; Prinz, D.; Amann-Hildebrand, A.; Krooss, B. M.; Pipich, V. On the Use and Abuse of N2 Physisorption for the Characterization of the Pore Structure of Shales; 2016; pp 151–161. https://doi.org/10.1346/CMS-WLS-21.12.
(47) Shindo, D.; Oikawa, T. Energy Dispersive X-Ray Spectroscopy. In *Analytical Electron Microscopy for Materials Science*; Shindo, D., Oikawa, T., Eds.; Springer Japan: Tokyo, 2002; pp 81–102. https://doi.org/10.1007/978-4-431-66988-3_4.
(48) Russ, J. C. *Fundamentals of Energy Dispersive X-Ray Analysis*; Butterworths monographs in materials; Butterworths: London Boston, 1984.
(49) Vernon-Parry, K. D. Scanning Electron Microscopy: An Introduction. *III-Vs Rev.* **2000**, *13* (4), 40–44. https://doi.org/10.1016/S0961-1290(00)80006-X.
(50) Holmes-Hampton, G. P.; Tong, W.-H.; Rouault, T. A. Biochemical and Biophysical Methods for Studying Mitochondrial Iron Metabolism. In *Methods in Enzymology*; Elsevier, 2014; Vol. 547, pp 275–307. https://doi.org/10.1016/B978-0-12-801415-8.00015-1.
(51) de la Guardia, M.; Armenta, S. Multianalyte Determination Versus One-at-a-Time Methodologies. In *Comprehensive Analytical Chemistry*; Elsevier, 2011; Vol. 57, pp 121–156. https://doi.org/10.1016/B978-0-444-53709-6.00006-9.

(52) Olesik, J. W. Elemental Analysis Using ICP-OES and ICP/MS. *Anal. Chem.* **1991**, *63* (1), 12A-21A. https://doi.org/10.1021/ac00001a711.
(53) Fultz, B.; Howe, J. M. *Transmission Electron Microscopy and Diffractometry of Materials*, 4th ed.; Graduate texts in physics; Springer: Heidelberg ; New York, 2013.
(54) Tang, C. Y.; Yang, Z. Transmission Electron Microscopy (TEM). In *Membrane Characterization*; Elsevier, 2017; pp 145–159. https://doi.org/10.1016/B978-0-444-63776-5.00008-5.
(55) Gartner, L. P. *Textbook of Histology*, Fifth edition.; Elsevier: Philadelphia, PA, 2021.
(56) Shindō, D.; Oikawa, T. *Analytical Electron Microscopy for Materials Science*; Springer: Tokyo ; Berlin, 2002.
(57) Pednekar, P. P.; Godiyal, S. C.; Jadhav, K. R.; Kadam, V. J. Mesoporous Silica Nanoparticles: A Promising Multifunctional Drug Delivery System. In *Nanostructures for Cancer Therapy*; Elsevier, 2017; pp 593–621. https://doi.org/10.1016/B978-0-323-46144-3.00023-4.
(58) Rosqvist, E. Nanostructured Polymeric Surfaces for Biological Interfaces, Åbo Akademi, Turku, Finland, 2021.
(59) Hameed, B. S.; Bhatt, C. S.; Nagaraj, B.; Suresh, A. K. Chromatography as an Efficient Technique for the Separation of Diversified Nanoparticles. In *Nanomaterials in Chromatography*; Elsevier, 2018; pp 503–518. https://doi.org/10.1016/B978-0-12-812792-6.00019-4.
(60) Gaspari, F. 2.4 Thin Films. In *Comprehensive Energy Systems*; Elsevier, 2018; pp 88–116. https://doi.org/10.1016/B978-0-12-809597-3.00214-5.
(61) FINITE-SIZE CORRECTIONS FOR 4-POINT PROBE MEASUREMENTS.Pdf.
(62) Eden, R. ENTEROBACTERIACEAE, COLIFORMS AND E. COLI | Classical and Modern Methods for Detection and Enumeration. In *Encyclopedia of Food Microbiology*; Elsevier, 2014; pp 667–673. https://doi.org/10.1016/B978-0-12-384730-0.00097-5.
(63) Fuller, T. F.; Harb, J. N. *Electrochemical Engineering*, First edition.; Wiley: Hoboken, NJ, USA, 2018.
(64) Elgrishi, N.; Rountree, K. J.; McCarthy, B. D.; Rountree, E. S.; Eisenhart, T. T.; Dempsey, J. L. A Practical Beginner's Guide to Cyclic Voltammetry. *J. Chem. Educ.* **2018**, *95* (2), 197–206. https://doi.org/10.1021/acs.jchemed.7b00361.
(65) Behravesh, E.; Kumar, N.; Balme, Q.; Roine, J.; Salonen, J.; Schukarev, A.; Mikkola, J.-P.; Peurla, M.; Aho, A.; Eränen, K.; Murzin, D. Yu.; Salmi, T. Synthesis and Characterization of Au Nano Particles Supported Catalysts for Partial Oxidation of Ethanol: Influence of Solution PH, Au Nanoparticle Size, Support Structure and Acidity. *J. Catal.* **2017**, *353*, 223–238. https://doi.org/10.1016/j.jcat.2017.07.014.
(66) Lund, S.; Björnvik, E.; Wang, Q.; Wang, X.; Vajrave, S.; Wey, L. T.; Allahverdiyeva, Y.; Kauppila, J.; Smått, J.-H.; Peltonen, J.; Latonen, R.-M.; Lindfors, T. *Shear Exfoliated Few-Layer Graphene and Cellulose Nanocrystal Composite as Biocompatible Anode with Efficient Charge Transfer*.
(67) McCrory, C. C. L.; Jung, S.; Peters, J. C.; Jaramillo, T. F. Benchmarking Heterogeneous Electrocatalysts for the Oxygen Evolution Reaction. *J. Am. Chem. Soc.* **2013**, *135* (45), 16977–16987. https://doi.org/10.1021/ja407115p.
(68) Pasta, M.; La Mantia, F.; Cui, Y. Mechanism of Glucose Electrochemical Oxidation on Gold Surface. *Electrochimica Acta* **2010**, *55* (20), 5561–5568. https://doi.org/10.1016/j.electacta.2010.04.069.
(69) Sugano, Y.; Latonen, R.-M.; Akieh-Pirkanniemi, M.; Bobacka, J.; Ivaska, A. Electrocatalytic Oxidation of Cellulose at a Gold Electrode. *ChemSusChem* **2014**, *7* (8), 2240–2247. https://doi.org/10.1002/cssc.201402139.

7 Appendix

Table A. 1 : Optimization parameters of graphite/SC exfoliation trials. Parameters include the graphite type, rotor speed (*N*), length of exfoliation (*t*), duration of dialysis, number of water changes, the graphene concentration before the dialysis and the graphene concentration after the dialysis.

Graphite type	Rotor speed; *N* (RPM)	Length of exfoliation; *t* (h)	Duration of dialysis (h)	Number of water changes	Pre-dialysis concentration ($mg \cdot mL^{-1}$)	Post-dialysis concentration ($mg \cdot mL^{-1}$)
Sigma-Aldrich	$9.90 \cdot 10^3$	2.00	19	1	0.92	0.78
Finnish	$16.5 \cdot 10^3$	2.00	22	2	2.91	0.66
Alfa-Aesar	$13.0 \cdot 10^3$	2.00	22	2	2.48	0.19
Alfa-Aesar	$13.0 \cdot 10^3$	2.00	20	1	2.17	0.42
Alfa-Aesar	$13.0 \cdot 10^3$	2.50	19	0	2.78	0.45

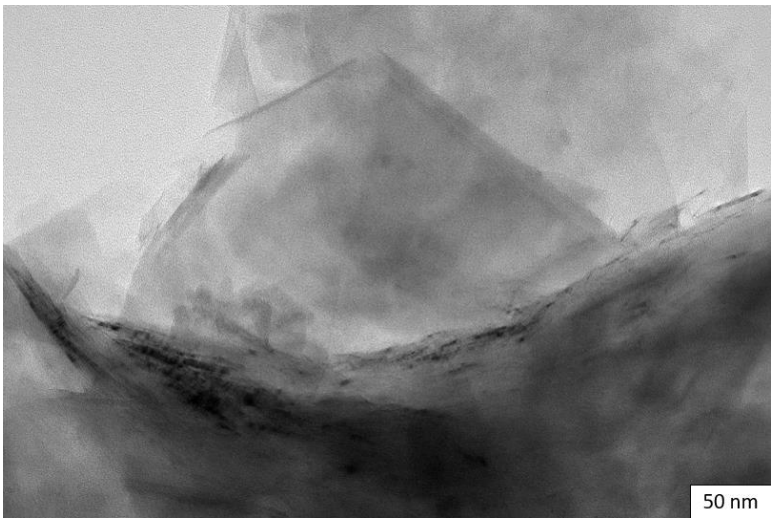

Figure A.1: TEM image of the pure graphene/SC dispersion.

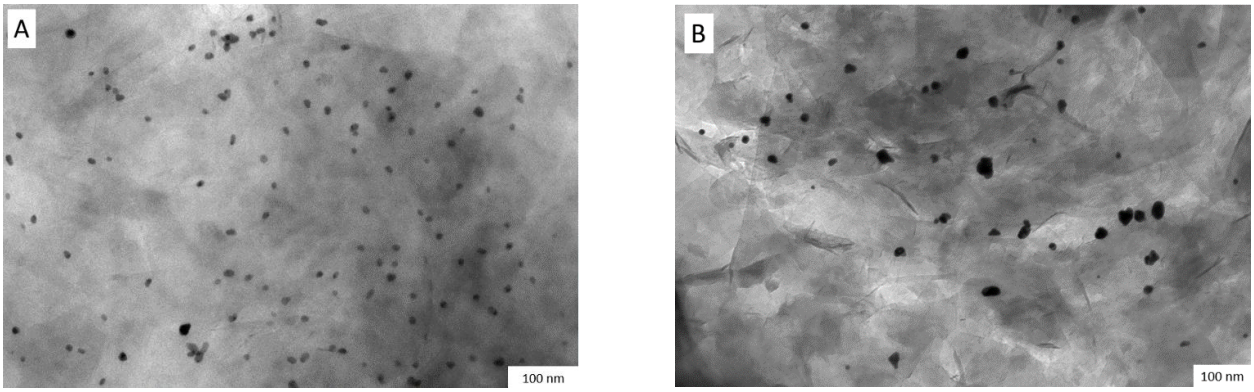

Figure A. 2: TEM images of graphene/AuNPs composite with a) AuNPs loaded after dialysis and b) AuNPs loaded before dialysis.

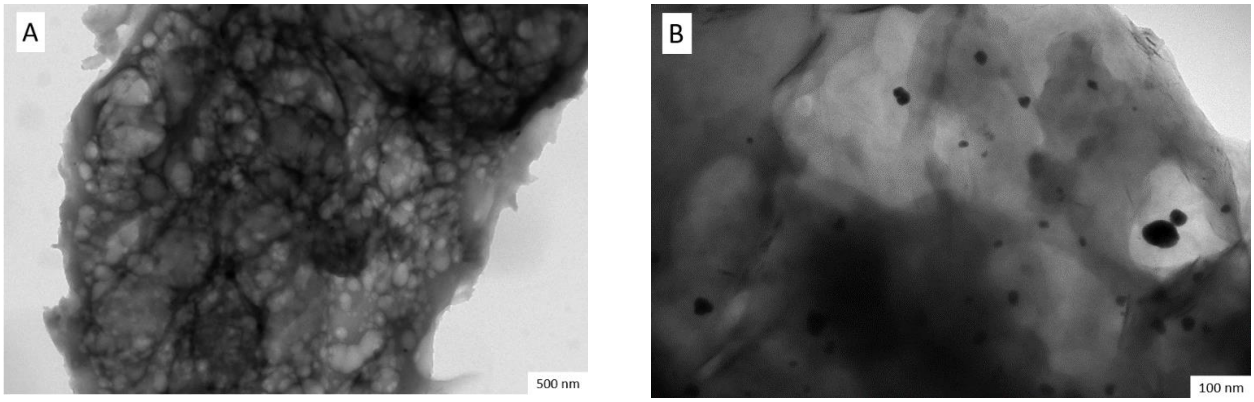

Figure A. 3: TEM images of hollowed structures throughout the graphene/ AuNPs where the AuNPs were loaded before the dialysis a) throughout the composite and b) impregnated with the AuNPs.

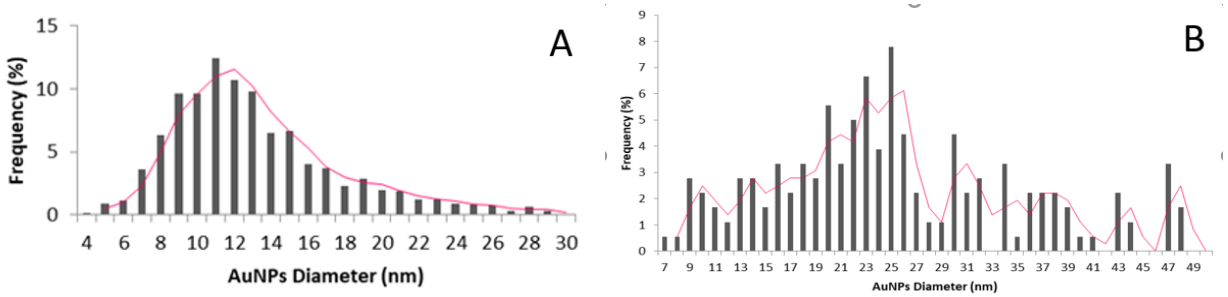

Figure A. 4: Particle size distribution (particle diameter in nm) of the AuNPs loaded a) after the dialysis and b) before the dialysis.